1972

Effects of CR-plating and environment on the cracking of low alloy steels at high temperatures

Robert C. Tooke

EFFECTS OF CR-PLATING AND ENVIRONMENT ON THE CRACKING OF LOW ALLOY STEELS AT HIGH TEMPERATURES

by

ROBERT C. TOOKE, 1941-

A DISSERTATION

Presented to the Faculty of the Graduate School of the

UNIVERSITY OF MISSOURI-ROLLA

In Partial Fulfillment of the Requirements for the Degree

DOCTOR OF PHILOSOPHY

in

METALLURGICAL ENGINEERING

1972

T. J. O'Keefe
Advisor

William A. Fraad

W. J. James

L. C. Moore

PUBLICATION DISSERTATION OPTION

This dissertation has been prepared in the style utilized by Metallurgical Transactions. Pages 1-46 will be presented for publication in that journal.

ABSTRACT

The cracking of low alloy Cr-Mo-V steels under cyclic stress at 1000-1100°C. was studied using a specially designed test apparatus. The results obtained from specimens plated with hard chromium are compared to those of unplated specimens. Tests conducted in gas mixtures of carbon monoxide and carbon dioxide showed that a high CO/CO_2 ratio retards cracking in both plated and unplated specimens. Both external and internal oxidation are used to explain these results. Inherent microcracks in the hard chromium plating promoted cracking in all CO/CO_2 environments. It was also found that these steels are severely embrittled in the presence of liquid copper.

ACKNOWLEDGEMENTS

The author wishes to thank his advisor Dr. Thomas J. O'Keefe, Professor of Metallurgical Engineering and Senior Investigator - Materials Research Center, for his valuable contributions throughout this investigation.

This research was performed as a portion of contract DAAF01-69C-0541 administered by the Science and Technology Laboratory of the U. S. Army Weapons Command, Rock Island Arsenal, Rock Island, Illinois.

TABLE OF CONTENTS

LIST OF ILLUSTRATIONS

LIST OF TABLES

I. INTRODUCTION

Cracks which develop in low caliber, rapid fire machine gun barrels provided the impetus for this investigation. Such cracks limit the performance of these barrels and may lead to catastrophic failure such as that shown in Figure 1. The general subject of gun erosion has been reviewed in two major volumes.[1,2] Although the possible influence of chemical environments on the formation and propagation of cracks has been recognized, many previous studies indicate the primary cause for such cracks is related to thermal-mechanical effects. In a recent investigation by the authors,[3] extensive metallurgical analyses were performed on several test fired 7.62 mm gun barrels. In barrels which contained a bore treatment of wear resisting, hard chromium plating, crack initiation was found to be connected with the microcracks inherent in the hard chromium electrodeposits. This condition is displayed in Figures 2 and 3. Crack initiation in the unplated barrels was delayed in comparison to the plated barrels.

It was concluded in the above investigation that chemical effects assumed major responsibility for cracking. The present study was undertaken therefore in an attempt to isolate the candidate chemical effects of CO/CO_2 gas

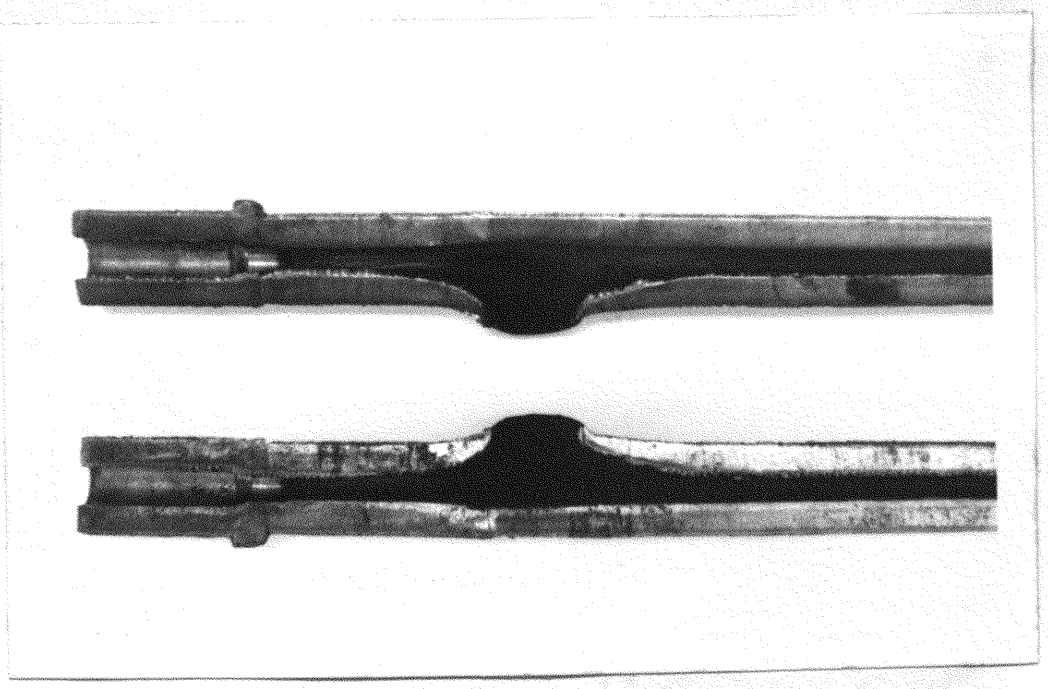

Figure 1. Catastrophic failure in 7.62 mm gun barrel.

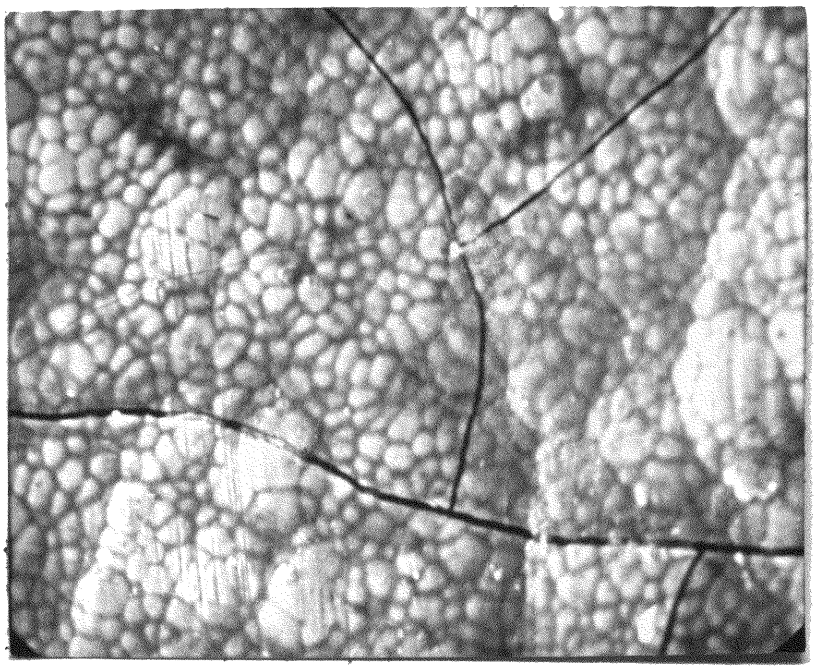

Figure 2. Inherent cracks in chromium plating. Scanning electron micrograph of bore surface.[3] 1000X

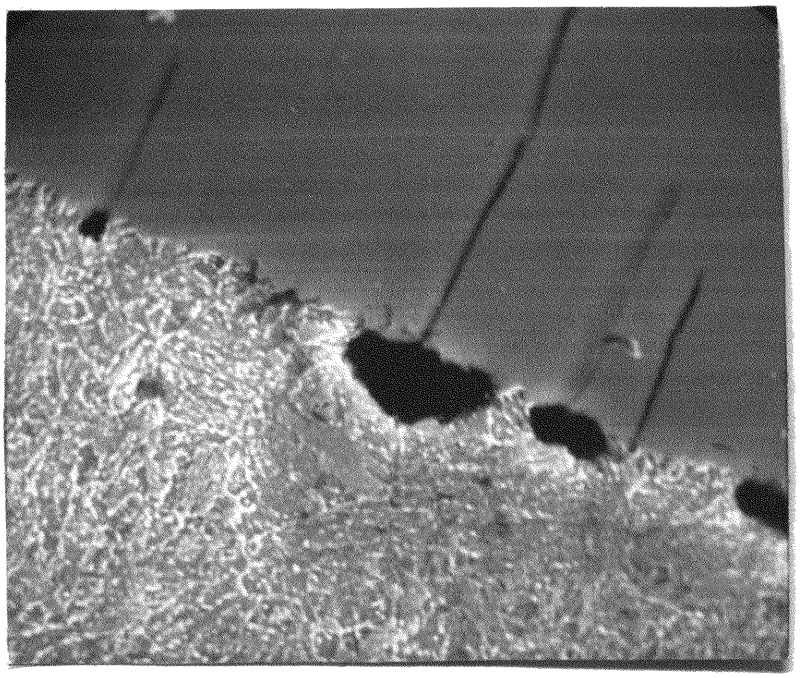

Figure 3. Initial attack of steel at base of cracks in Cr plating after only 10 rounds.[3] Scanning electron micrograph, nital etch. 10,000X

compositions and copper on the cracking of the low alloy, Cr-Mo-V steel (both Cr plated and unplated) at elevated temperature.

The effect of gas composition is of interest because an altered zone, thought to be the result of gas-metal reaction, has been observed around the cracks. Carbon monoxide and carbon dioxide are major components of spent propellent and a high CO/CO_2 ratio has been reported to be desirable.[1,2]

Alloys of iron and carbon will react with the above gases as follows:

$$Fe + CO_2 = FeO + CO \qquad (I)$$

$$2CO = \underline{C} + CO_2 \qquad (II)$$

Using the values given by Gurry,[4] for the equilibrium constants K_I and K_{II}, and the activity of carbon in austenite, $A\underline{c}$, the equilibrium gas compositions for the two reactions have been calculated for 1000°C (Figure 4).

Several additional factors must be considered in the oxidation of alloy steels and this makes analysis of the mechanisms of oxidation considerably more complex. The general subject of alloy oxidation has been treated in many reviews.[5-7] It is also known that alloying elements affect the carburizing behavior of steels. Chipman and Brush report a decrease in the $A\underline{c}$ at 1000°C in the

presence of the alloying elements of Cr, Mo, V, and Mn which would shift the equilibrium line for reaction II to the right in Figure 4.

The effect of copper was selected for study because it was detected in the cracks of the test fired barrels. The observation of copper in the cracks is of significance because the tendency of liquid copper and copper base alloys to penetrate the grain boundaries of steel is well known.[9-12]

A search of the literature yielded no information of similar studies on low alloy steels in the vicinity of 1000°C. High strain fatigue tests on low alloy Cr-Mo-V steels at temperatures up to 700°C have been performed by Coles, et al.,[13] Hill,[14] and Krempl and Walker.[15] Environmental conditions, specifically those contributing to oxidation, are postulated as possible factors in the mechanism of failure in each of these investigations. Numerous other studies have been concerned with the effect of gaseous environments on crack initiation and propagation in a variety of alloys under cyclic stress at elevated temperature.[16-21] Summarizing the results, tests performed in a vacuum were generally superior to those in air. In some cases crack nucleation was associated with pronounced localized oxidation and subsequent intergranular crack propagation was accompanied by oxidation or attributed to oxygen adsorption.

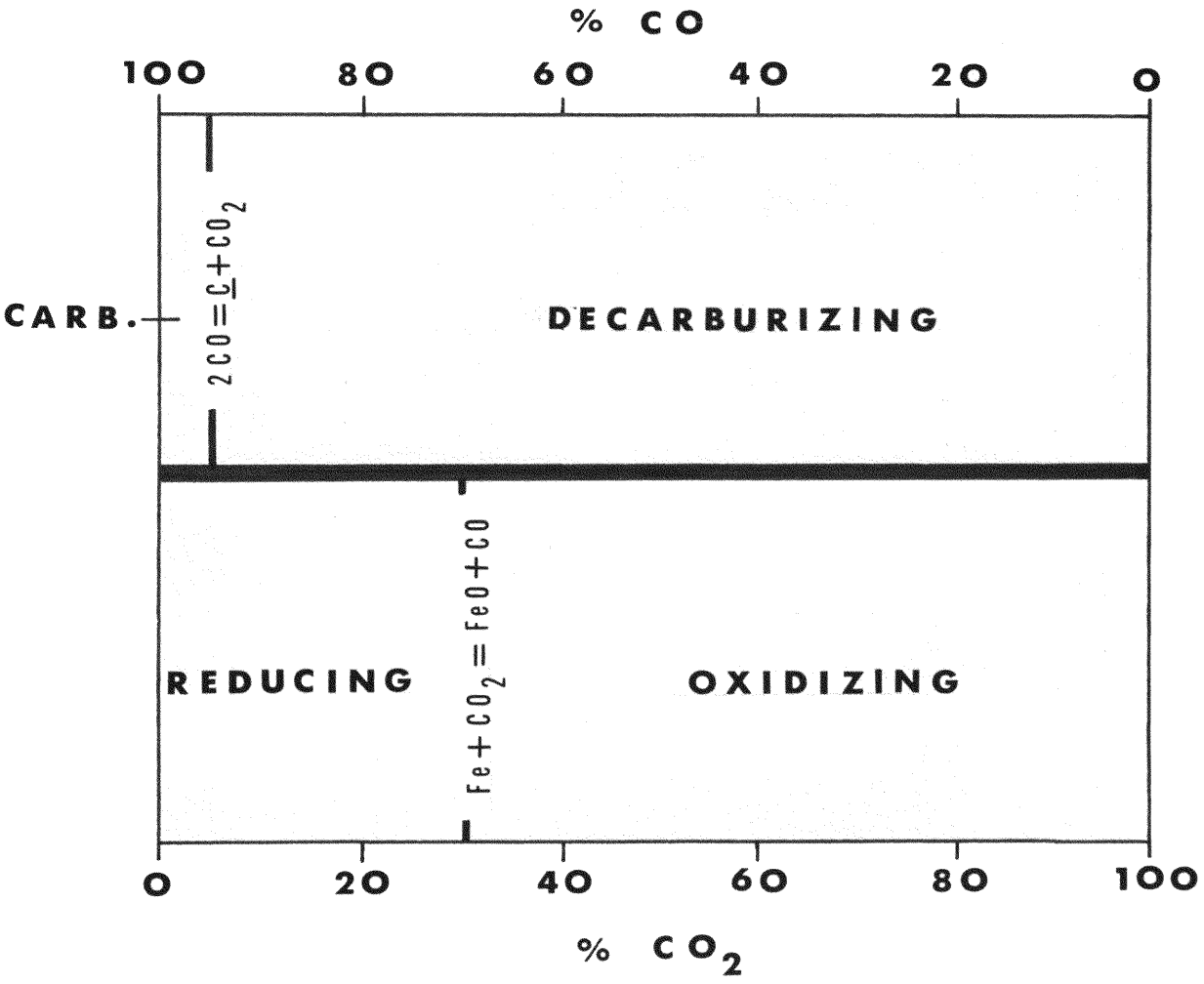

$Fe + CO_2 = FeO + CO$ $\quad K = P_{CO}/P_{CO_2}$ $\quad K @ 1000°C = 2.5$

$CO = \underline{C} + CO_2$ $\quad K = (P_{CO_2})(A_{\underline{C}}/P^2_{CO})$ $\quad K @ 1000°C = .067$

$A_{\underline{C}}$ for .45% C = .21

Figure 4. Reactions of iron with CO/CO_2 atmospheres.[5]

II. EXPERIMENTAL DETAILS

The apparatus employed in this investigation is shown in Figures 5 and 6. It was designed to permit high strain, reverse bending tests at elevated temperature in controlled atmospheres. The test specimen, described below, was contained in a vacuum-tight chamber, induction heated to the desired temperature and alternately stressed in tension and compression as a cantilever beam. The unique feature of this apparatus was the incorporation of electromagnets to provide the desired stress. This was accomplished by switching the power between two diametrically opposite electromagnets thereby attracting the extension rod to first one side and then the other. The extent of travel, i.e. the stress amplitude, was limited by the stops attached to the bottom plate of the test chamber. No attempt was made to determine the actual plastic strain involved in these experiments.

Two types of specimens were used, both of which were of the dimensions indicated in Figure 7. After machining, the specimens were finished with 600 grit emery paper. Unplated specimens were finished to a gage section diameter of .200". Specimens to be plated were finished to a diameter of .192" and subsequently received a standard electrolytic hard chromium plating of a thickness of .003" to .004". All specimens were made from forged stock from

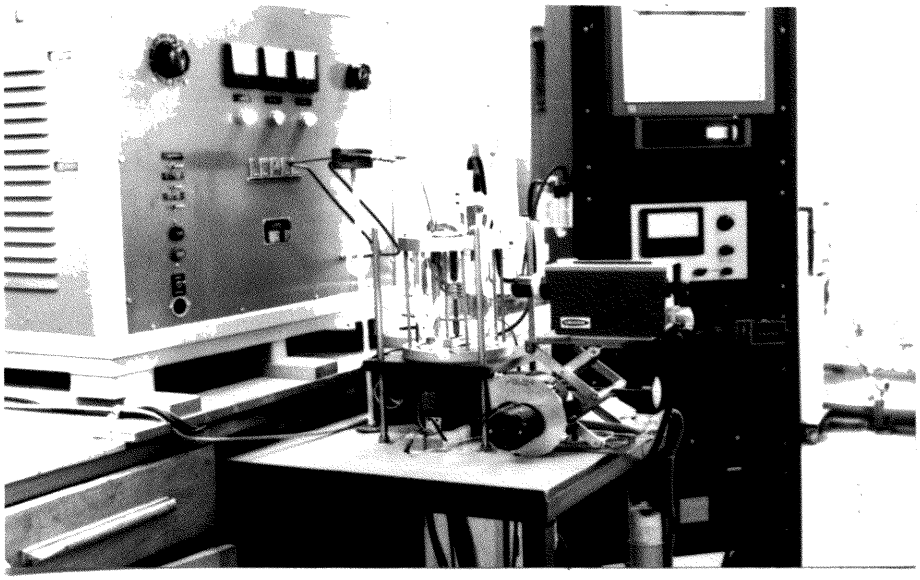

Figure 5. Photograph of apparatus.

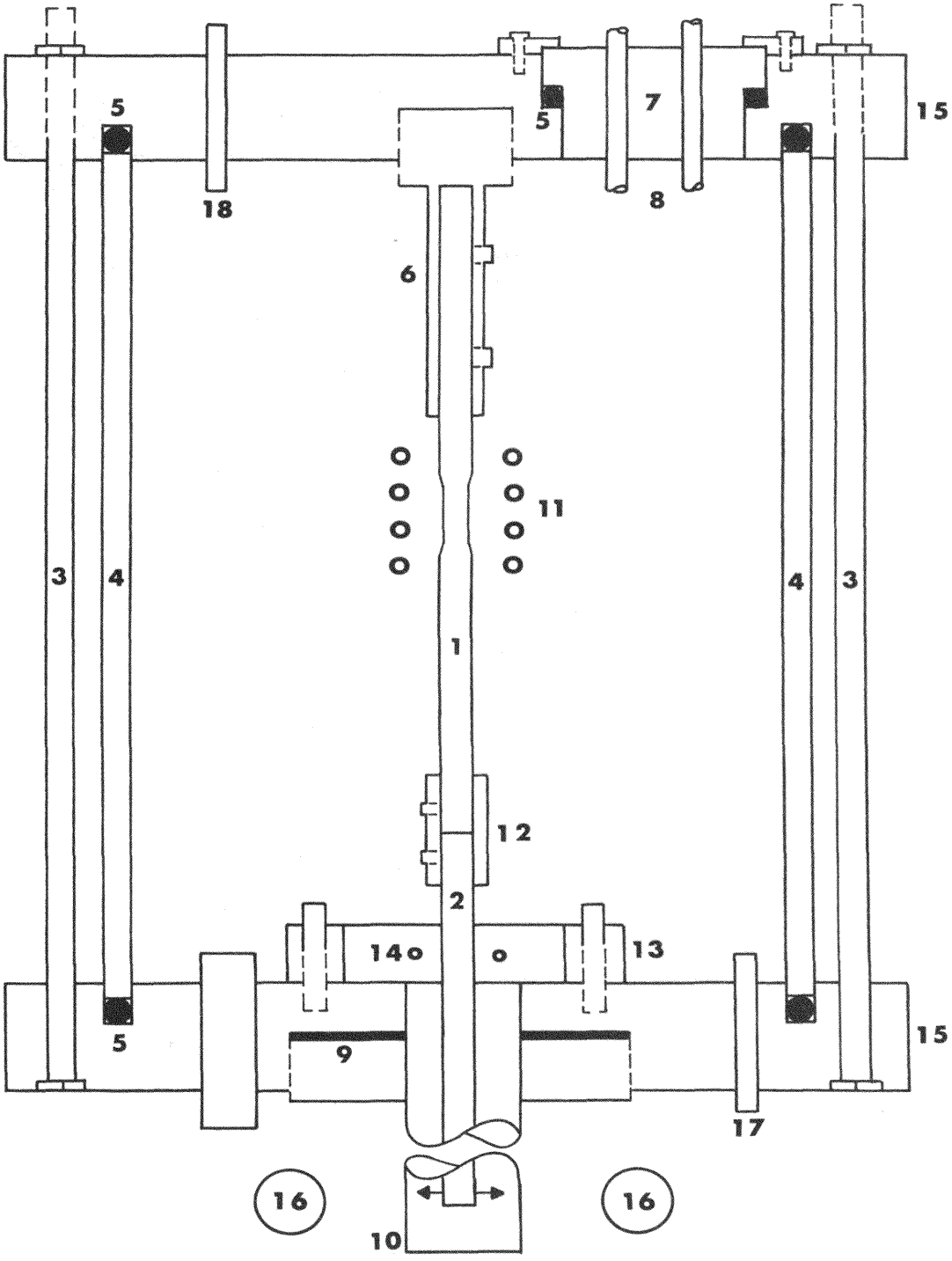

Figure 6. Test Chamber. 1. specimen 2. specimen extension rod 3. tie rods 4. glass 5. O rings 6. support stud 7. plexiglass plug 8. induction coil leads 9. gasket 10. hand down tube 11. induction coil 12. coupler 13. specimen guide 14. stress stops 15. Al base and cap 16. electromagnets 17. gas in 18. gas out

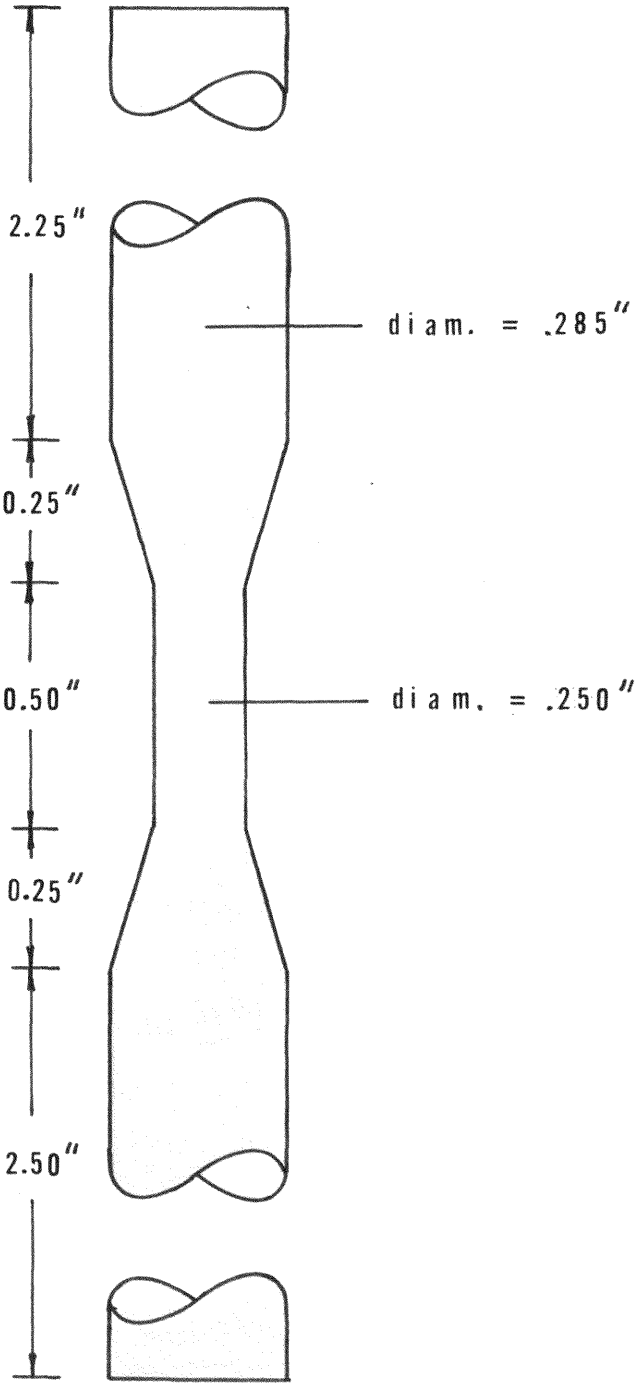

Figure 7. Test specimen dimensions.

the same bar of Cr-Mo-V steel with the following check analysis.

C	Mn	Si	Cr	Mo	V
0.43	0.97	0.29	1.29	0.65	0.21

Temperature was automatically controlled with measurement being made with an infrared radiation pyrometer. Because of changing specimen surface conditions, it was necessary to create a blackbody condition by means of a hole drilled in the sample. This temperature control hole was outside the gage section of the specimen so as not to interfere with the stress distribution during testing. Temperature gradients along the test specimen were determined to establish the relationship between the control temperature and the actual temperature in the gage section. Calibration of the radiation pyrometer involved comparison with temperatures measured by a Pt-Pt 10% Rh thermocouple inserted next to the hole and further checked by observing the melting temperature of Ag and Cu. Temperature accuracy was judged to be better than ± 10°C at 1000°C.

The atmosphere in the test chamber was established through the use of high purity compressed gases of argon (99.996%), carbon monoxide (99.7) and carbon dioxide (99.9). Gas flowrate, 44 cc/min, and mixing of the gases was monitored on a gas proportioner which blended the

gases by individual flowmeters. All gas mixtures were analyzed with a gas chromatograph.

Copper was placed on the designated specimens by melting a fine copper wire in situ at 1100°C in argon and allowing 15 seconds for the copper to flow over the surface before proceeding with the test. The liquid copper readily spread over both the steel and Cr plated surfaces.

Numerous factors were involved in the selection of the test temperature which was generally 1000°C. Actual bore temperatures are unknown. However, there was some evidence that copper was at, or near, its melting point in the test fired barrels. Furthermore, since flame temperatures of propellants are excessively high, it was desirable to make these tests at the highest temperature possible which allowed retention of some bulk strength integrity in the steel. Since a steep temperature gradient exists on the surfaces in contact with propellant gases, it should be noted that the test temperature is intended to be representative of only a thin zone surrounding a crack.

Preparation for a typical test included closing the test chamber after assembly of test specimens, evacuating, backfilling with the desired gas, re-evacuating, and allowing the gas to flow for 15 minutes. At this time the specimen was heated to the test temperature

(generally 1000°C) which required less than 60 seconds and cycling was begun. Most tests were carried to failure with the total number of cycles recorded by an impulse counter in the magnet circuit.

III. RESULTS

Tabulation of the cycles to failure as a function of environmental conditions is found in Table 1. Numerous other tests were made which were not carried to complete failure. Examples of failed specimens are shown in Figure 8. All test pieces failed in the upper end of the gage section which was located in the hottest part of the specimen. Figure 9 is a graphical presentation of the results contained in Table 1. An increase in the percent of carbon monoxide retarded failure in both types of specimens but the effect was more pronounced in the unplated specimens.

The chromium plated specimens were inferior in all ratios of CO and CO_2; however, in argon the cycles to failure for plated and unplated specimens are comparable.

In high CO_2 (>50%) gas mixtures, both plated and unplated specimens develop large oxide-filled pits which lead to cracking. Figures 10 and 11 depict this condition. As seen in Figure 10, the chromium remains intact with pits developing in the steel through the existing cracks in the Cr plating. The appearance after etching of a crack representative of those found in the high CO_2 specimens is shown in Figure 12. A white constituent, ferrite, representing decarburization, a dark etching mottled or oxygen-affected zone, and oxide lining the

TABLE I

EXPERIMENTAL DATA

Specimen	Environment	Temp. °C	Cycles to Failure
Cr plated	100% CO_2	1000	9,968
Cr plated	100% CO_2	1000	8,626
Cr plated	80% CO_2, 20% CO	1000	10,160
Cr plated	65% CO_2, 35% CO	1000	15,0217
Cr plated	50% CO_2, 50% CO	1000	12,955
Cr plated	50% CO_2, 50% CO	1000	17,400
Cr plated	35% CO_2, 65% CO	1000	14,822
Cr plated	20% CO_2, 80% CO	1000	15,092
Cr plated	20% CO_2, 80% CO	1000	23,716
Cr plated	15% CO_2, 85% CO	1000	26,106
Cr plated	10% CO_2, 90% CO	1000	27,853
Cr plated	100% CO	1000	19,875
Cr plated	100% CO	1000	28,831
Cr plated	100% CO	1000	31,266
Cr plated	100% CO	1000	26,806
Cr plated	100% Argon	1000	78,068
Cr plated	100% Argon	1000	74,132

TABLE I (continued)

Specimen	Environment	Temp. °C	Cycles to Failure
Unplated	100% CO_2	1000	17,791
Unplated	100% CO_2	1000	18,132
Unplated	80% CO_2, 20% CO	1000	22,158
Unplated	50% CO_2, 50% CO	1000	29,608
Unplated	50% CO_2, 50% CO	1000	35,324
Unplated	20% CO_2, 80% CO	1000	49,618
Unplated	20% CO_2, 80% CO	1000	38,572
Unplated	100% CO	1000	74,204
Unplated	100% CO	1000	68,009
Unplated	100% Argon	1000	75,350
Unplated	100% Argon	1100	>10,000
Unplated	Cu, 100% Argon	1100	39
Unplated	Cu, 100% Argon	1100	38
Cr plated	100% Argon	1100	>10,000
Cr plated	Cu, 100% Argon	1100	34
Unplated	Cu, 100% Argon	1000	>10,000

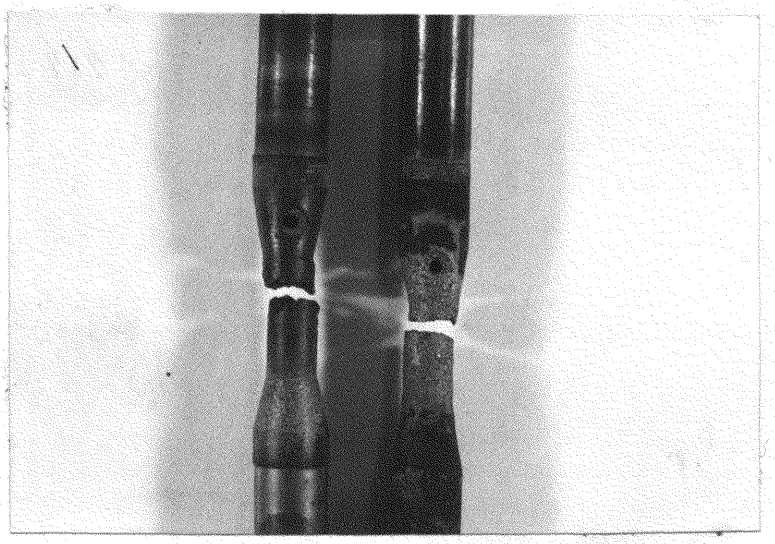

Figure 8. Test specimens after failure, right - unplated; left - Cr plated.

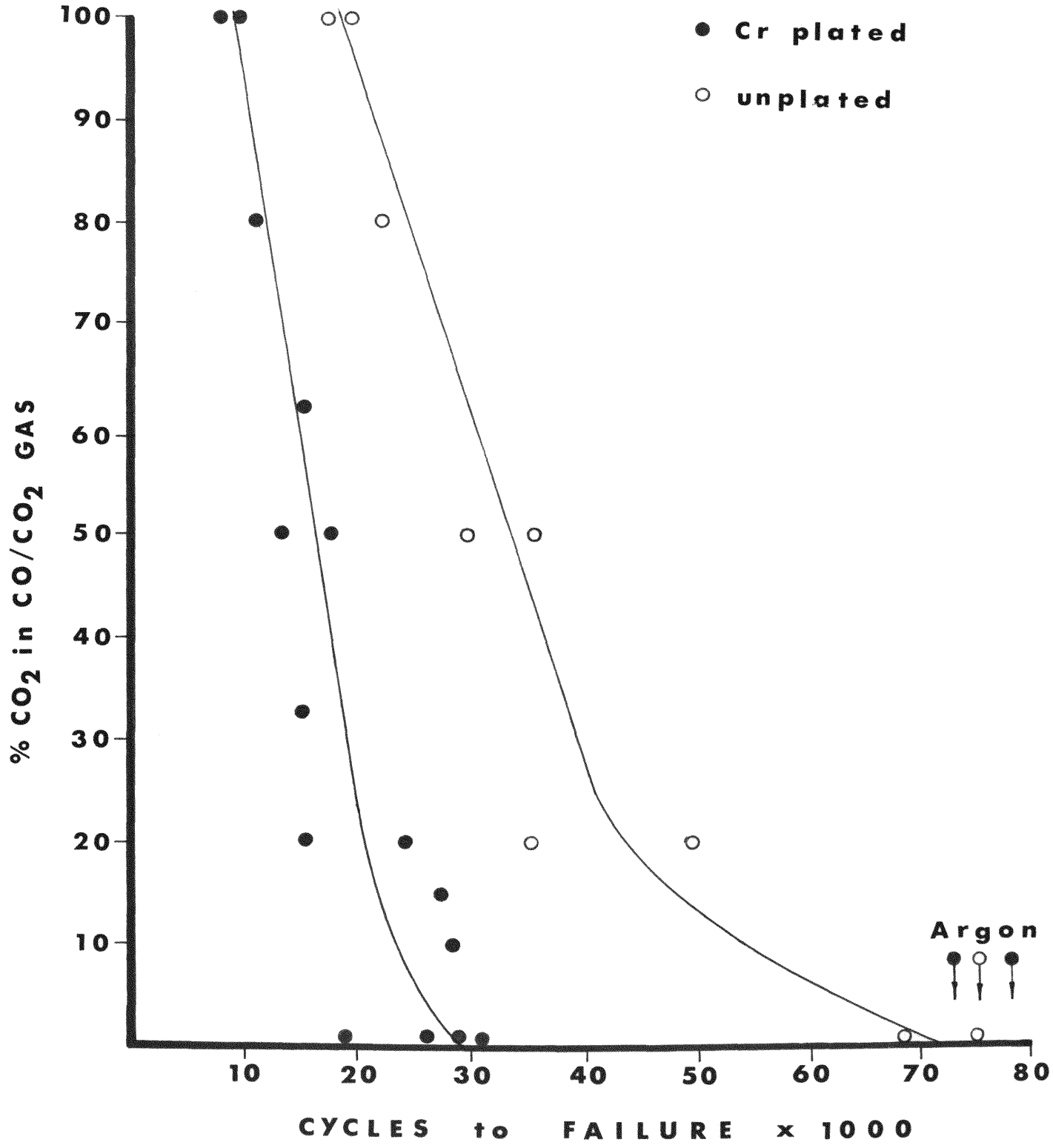

Figure 9. Cycles to failure for plated and unplated barrels in CO/CO_2 atmospheres.

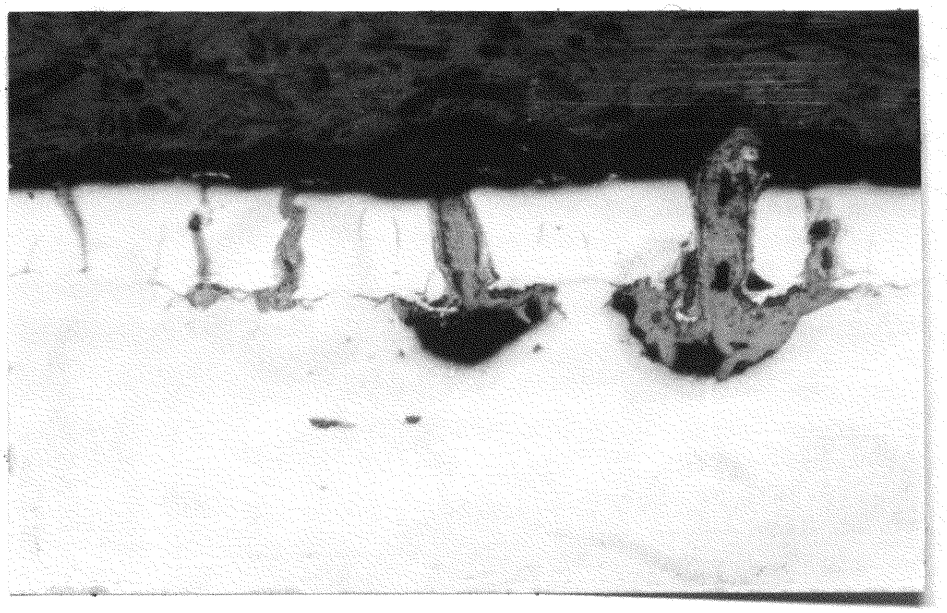

Figure 10. Pitting beneath Cr plating typical of high CO_2 mixtures, unetched. 200X

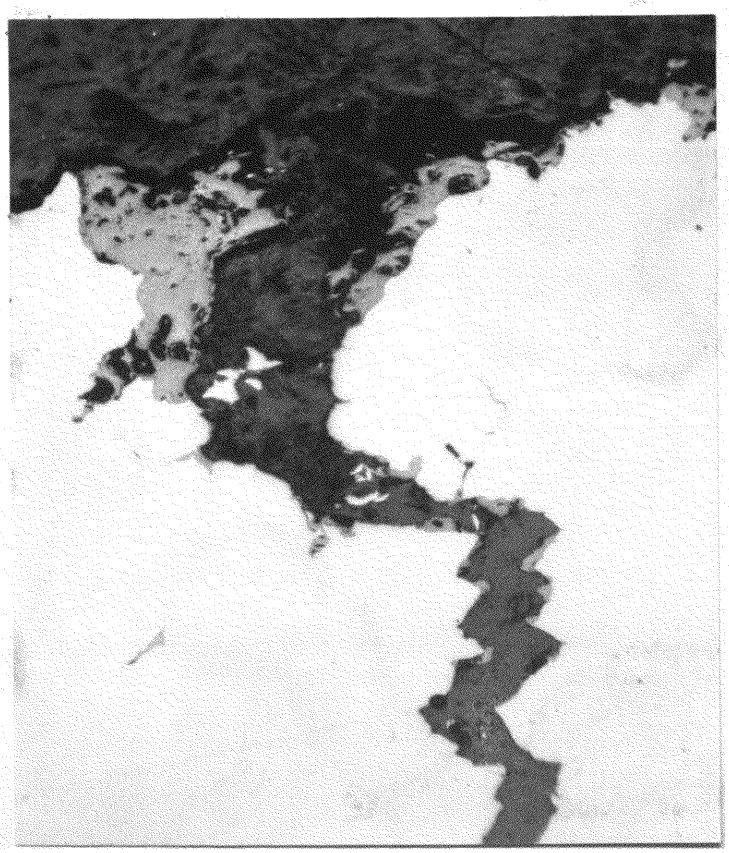

Figure 11. Oxide-filled crack generating from a pit in unplated sample, unetched. 100X

crack surfaces are all in evidence. Oxide, which filled or lined all of the cracks, is very much in evidence at high magnification, Figure 13, in the leading tip of the crack. The mottled zone in the base metal which is apparent in Figure 12 and even more clearly shown in Figure 13 was not observed in 100% CO_2 but gradually increased in size as the CO_2 content decreased from 80% to 50%. Decarburization of the steel also increased with decreasing CO_2 which is opposite to what was expected considering reaction II. However, scale formation is known to provide protection against decarburization of the steel substrate.[22]

Some oxide pits were observed at 50% CO_2, but below this point, cracking in the absence of pitting became increasingly prevalent. Figures 14 and 15 illustrate this condition. Oxide (scale) remained in abundance at 50% CO_2 but completely disappeared in 20% CO_2. In this range, and at 10% CO_2, the mottled zone in the steel became more developed, the particles in this zone grew larger, and a preference for grain boundary formation was noticed. Figure 16 shows this zone at 20% CO_2 near the surface of an unplated specimen. Figure 17 depicts the mottled zone at the root of a crack. This zone is characteristic of all surfaces exposed to the gas, including the fracture surface. Decarburization continued to increase from 50% to 20% CO_2. The unplated specimens exhibited few cracks in CO_2 contents of 50% or more. Some failed

Figure 12.

Photomicrograph of crack representative of high CO_2 specimens, nital etch. 500X

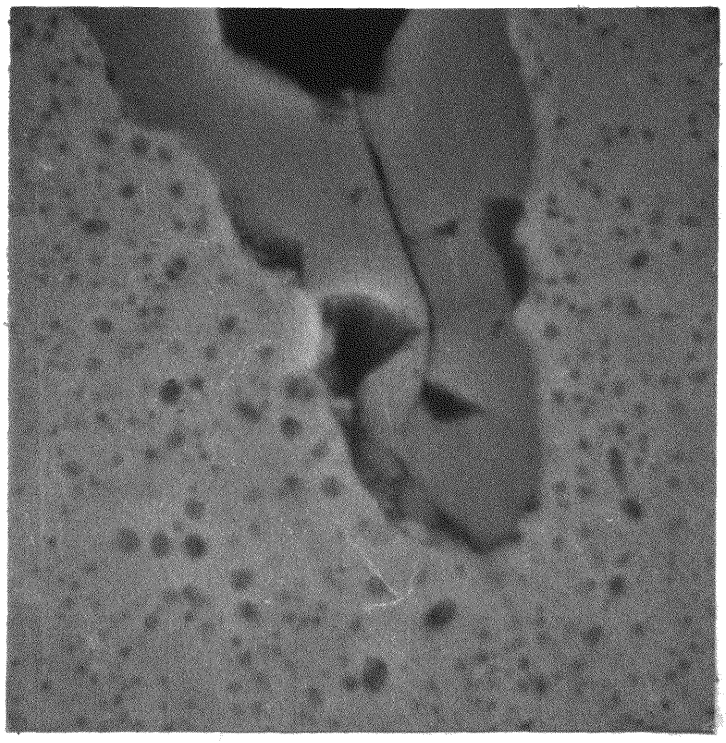

Figure 13.

Scanning electron micrograph showing oxide in crack and mottled zone. 80% CO_2, unetched. 3000X

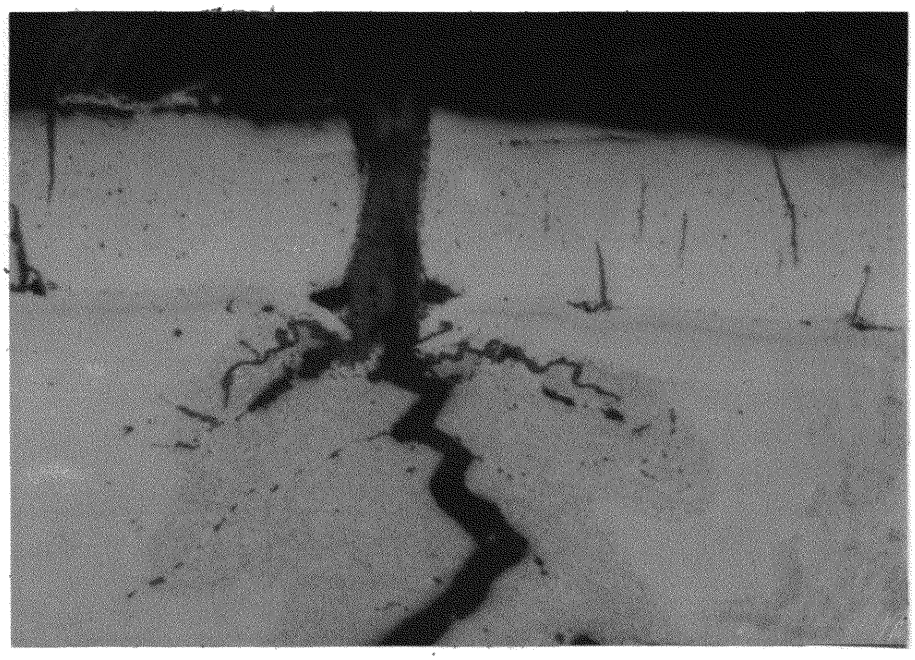

Figure 14. Crack propagation in the absence of pitting in Cr plated specimen. 50% CO_2, unetched. 500X

Figure 15. Crack propagation in the absence of pitting in Cr plated specimen. 50% CO_2, unetched. 200X

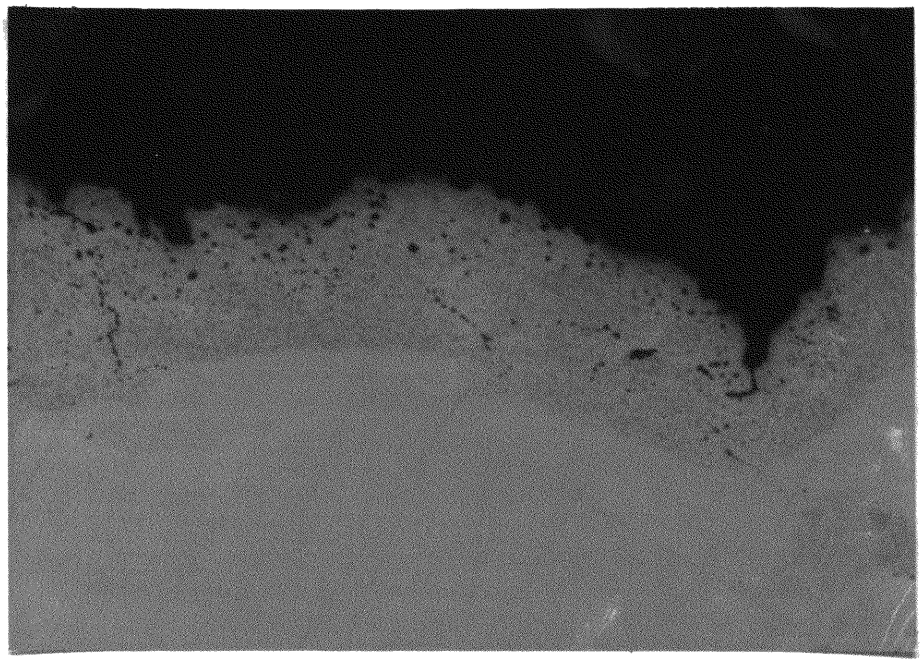

Figure 16. Mottled zone on surface of 20% CO_2 specimen. Note coarser particles nearer surface and intergranular particles. Unplated specimen, unetched. 500X

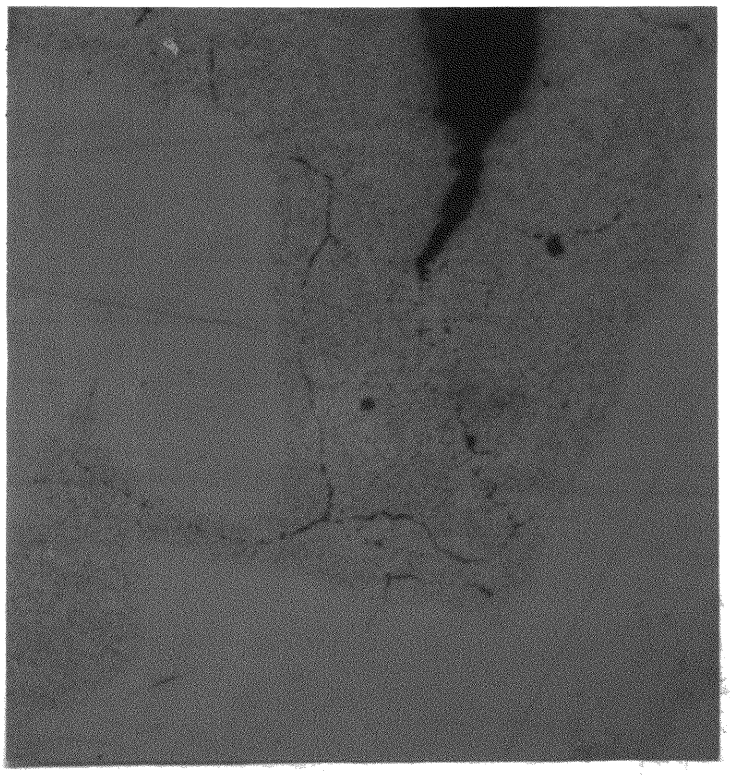

Figure 17. Intergranular formation of precipitate in mottled zone formed at crack tip, unetched. 750X

specimens had no secondary cracks, the only apparent damage being the introduction of the crack which propagated to complete failure. Contrasted to this, Cr plated specimens were always observed to contain numerous cracks.

Tests in 100% CO yielded cracks which in most cases were somewhat finer than those previously described. Again the mottled zone was apparent on the unetched sample, Figure 18. On etching, Figure 19, the structure was seen to be altered around the cracks. Microhardness determinations indicated this area to be softer than the martensitic matrix.

As seen in Figures 20 and 21, cracks appear to develop initially in the particles in the mottled zone and then cracking occurs between particles. The significance of the mottled zone suggested by Figures 20 and 21 dictated that an effort be made to identify the particles located in this zone. Utilizing the non-dispersive x-ray spectrometer accessory to a scanning electron microscope made it possible to obtain an elemental analysis of the particles since the electron beam could easily be focused on an individual particle. This resulted in detection (Figure 22) of the elements Fe, Cr, Mn, and V in the particles. Occasional traces of Mo were also detected. Only Fe and sometimes very small amounts of Cr were found in the matrix of the mottled zone. The relative amounts of the elements Cr, Mn, and V in a particle were observed to increase with decreasing % CO_2. These results were futher verified with

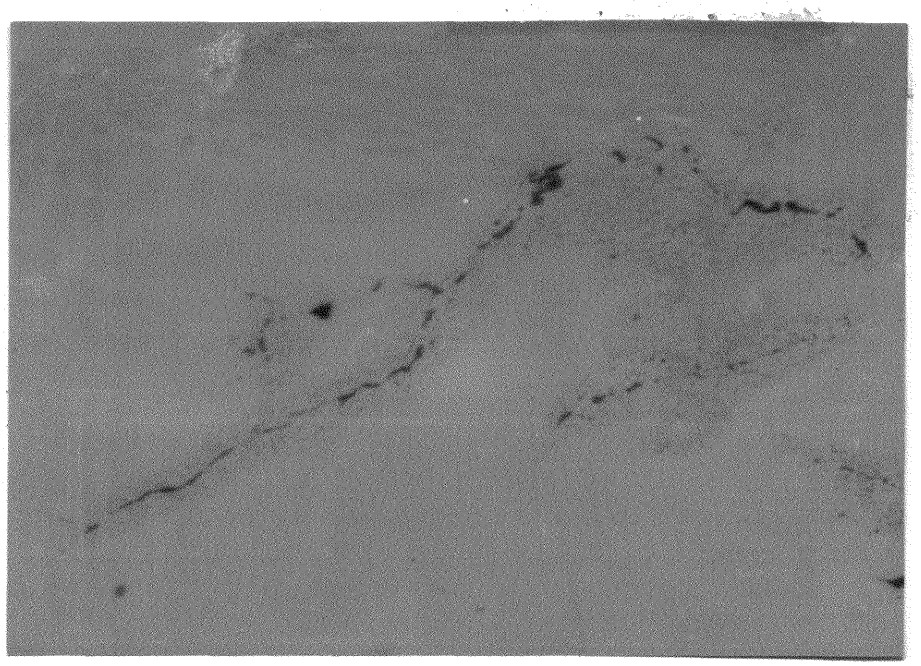

Figure 18. Fine crack in 100% CO specimen, unetched. 500X

Figure 19. Altered zone around crack in 100% CO specimen as distinguished from martensitic matrix by nital etch. 500X

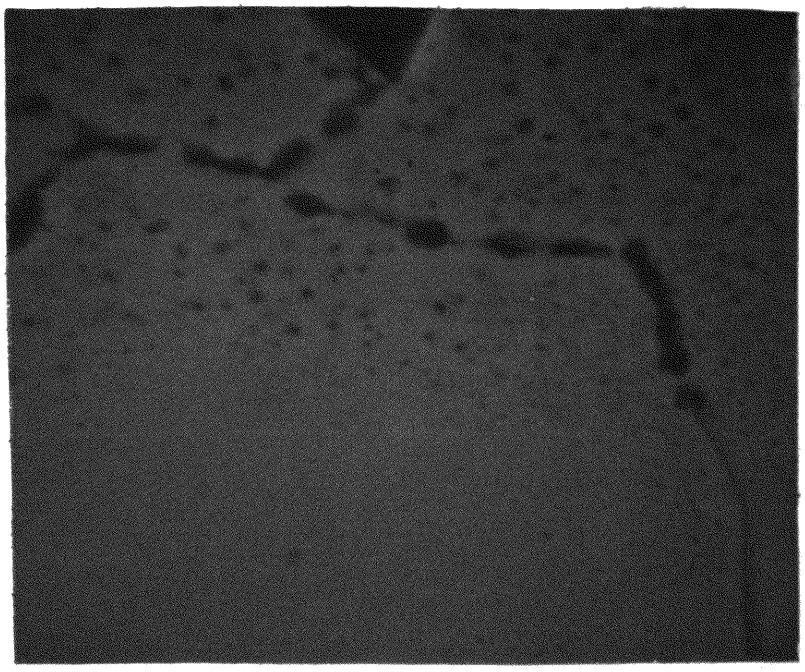

Figure 20. Scanning electron micrograph of mottled zone. Note crack following intergranular particles. Unetched. 3000X.

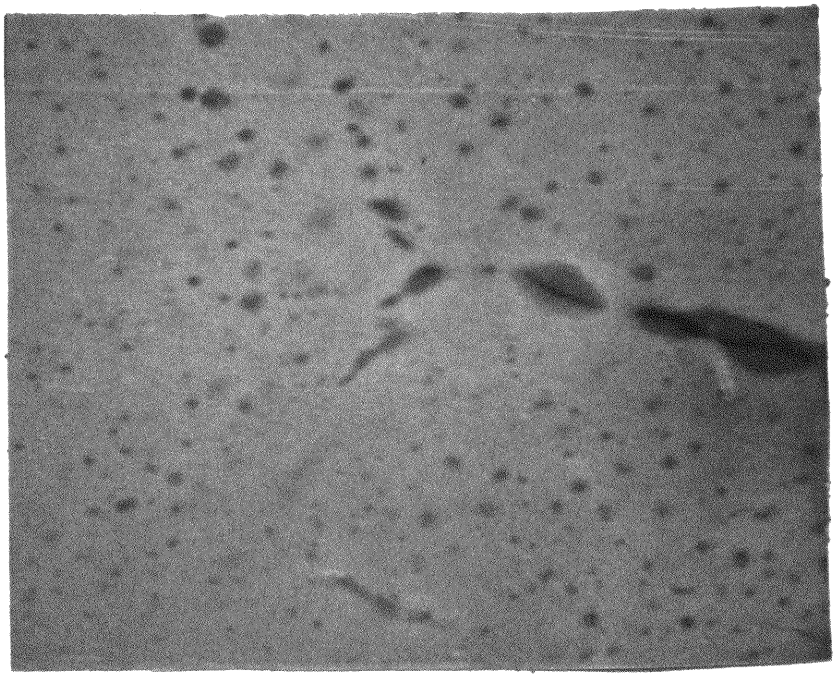

Figure 21. Scanning electron micrograph of mottled zone. Note cracking in the particles. Unetched. 3000X.

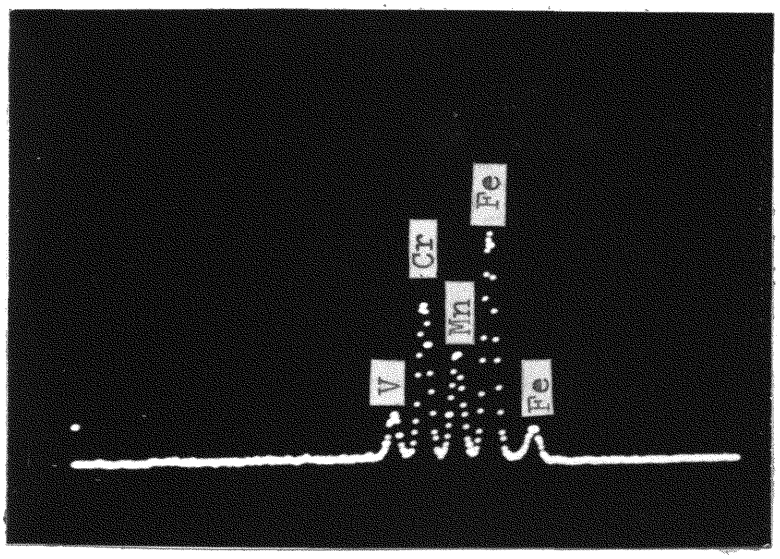

Figure 22. X-ray spectrometer analysis of precipitate particles in mottled zone.

the electron microprobe. X-ray scans produced discrete areas corresponding to the particles, which were high in Cr, Mn, and V. In addition, microprobe results established the mottled zone to be enriched in oxygen as shown in Figure 23A and 23B. No carbon concentration indicative of carburization was located.

Metallography was extended to the tests made in argon. The cracks, Figure 24, tended to be more blunt. A faint mottled zone was observed on most of the specimens but it diminished on the fracture surfaces. A two-layer diffusion zone formed between the steel and the Cr in all plated specimens. Cracking and separation were common along this zone which in some instances facilitated removal of the plating (Figure 24). These diffusion zones are shown in Figure 25 as they appear after testing in argon. Indenti-cal zones have been identified as the complex carbides $(Cr,Fe)_{23}C_6$ and $(Cr,Fe)_7C_3$.[23]

The topology of the fracture surfaces was studied with the SEM. High CO_2 contents results in gross scaling masking any detail. In the absence of scale formation, all fractures appeared similar, Figure 26 being representative.

Tests made in the presence of liquid copper required only 40 cycles before failure occurred. A thin film of copper covered the fracture surface. Figures 27 and 28 clearly show the extent of intergranular penetration of copper which is responsible for rapid failure. No difference between the Cr plated and unplated samples was

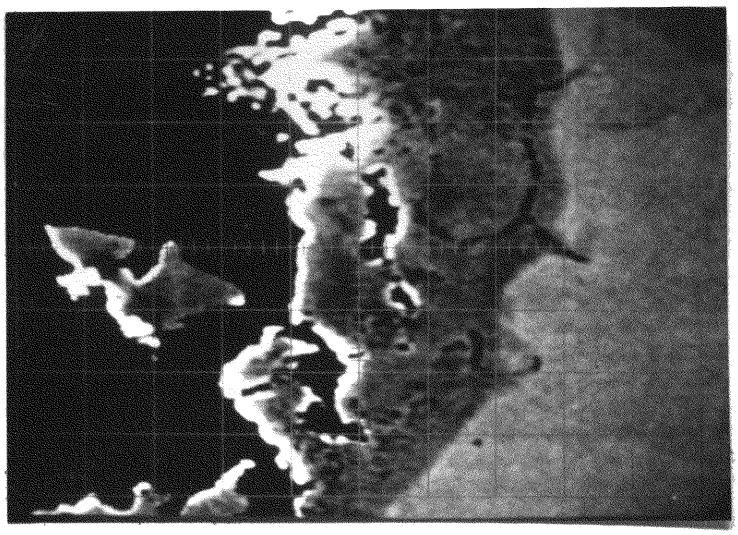

A

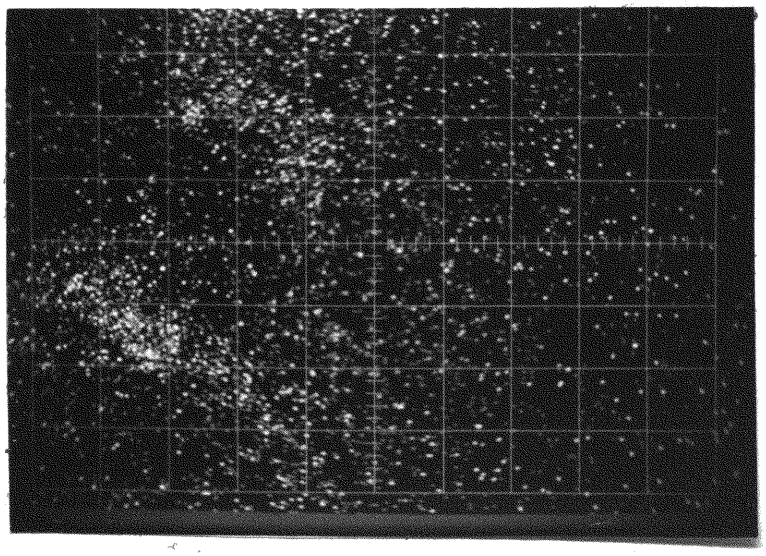

B

Figure 23. Electron microprobe results of the mottled zone. A. Electron image showing the zone to be of lower atomic number. B. Oxygen X-ray image indicating oxygen enrichment. 375X

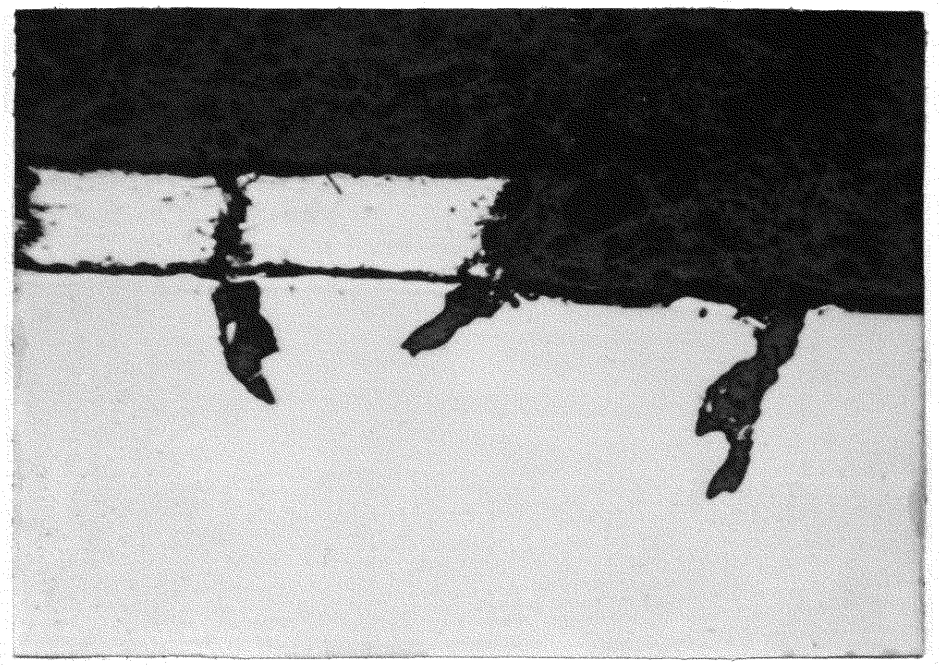

Figure 24. Blunt cracks in Cr plated specimen tested in argon. Unetched. 200X

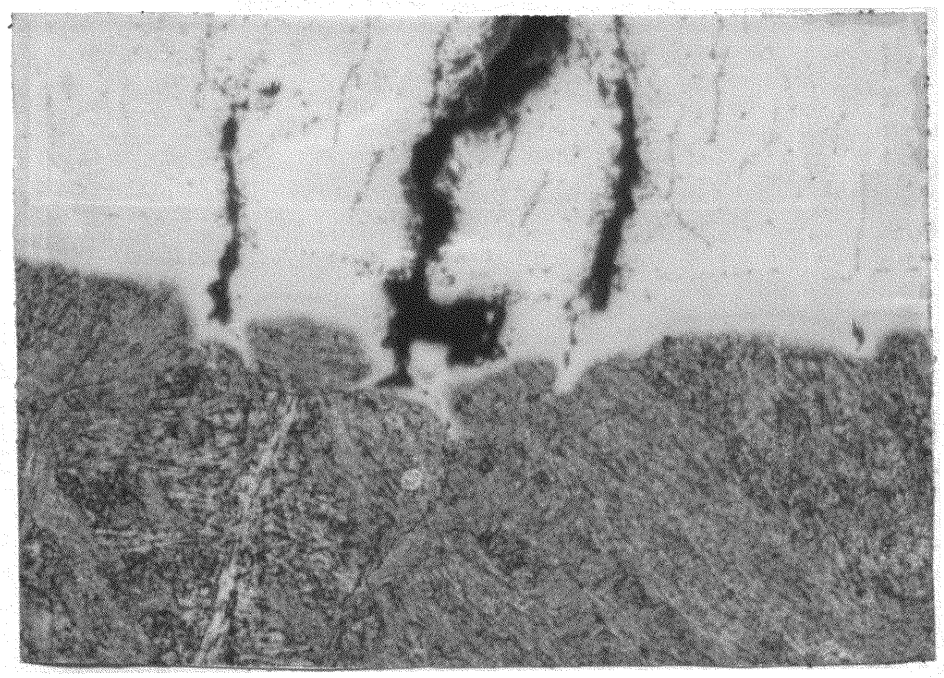

Figure 25. Diffusion zones formed in the Cr plated samples. Note two intermediate zones between Cr (top) and steel (bottom). Nital etch. 500X

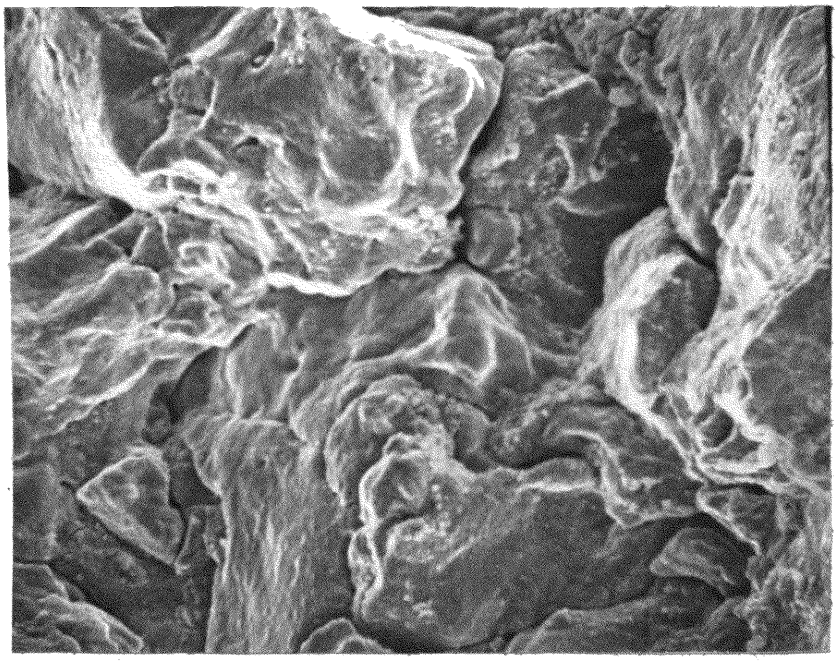

Figure 26. Scanning electron micrograph of fracture surface topology. 20% CO_2. 300X

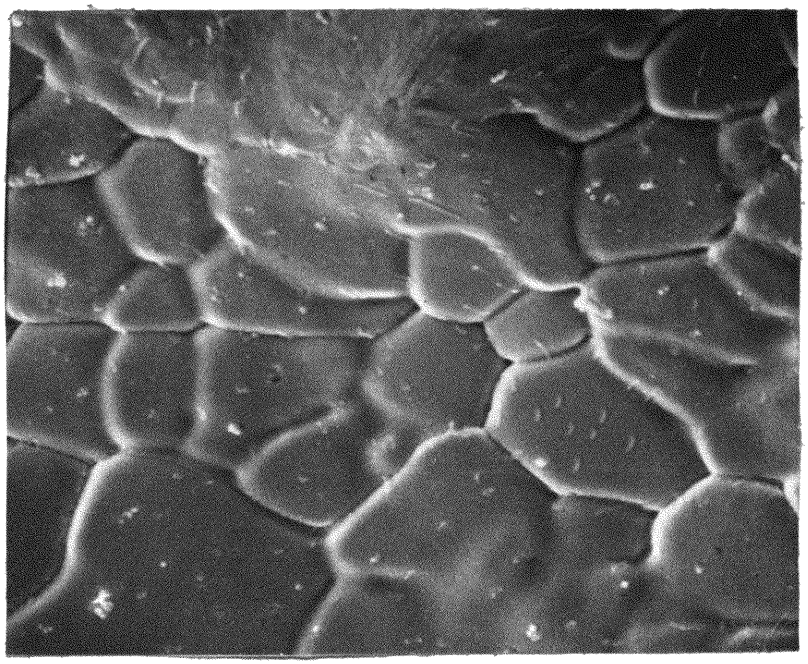

Figure 27. Scanning electron micrograph of Cu film over fracture surface. Note preferential attack of copper at grain boundaries. 600X

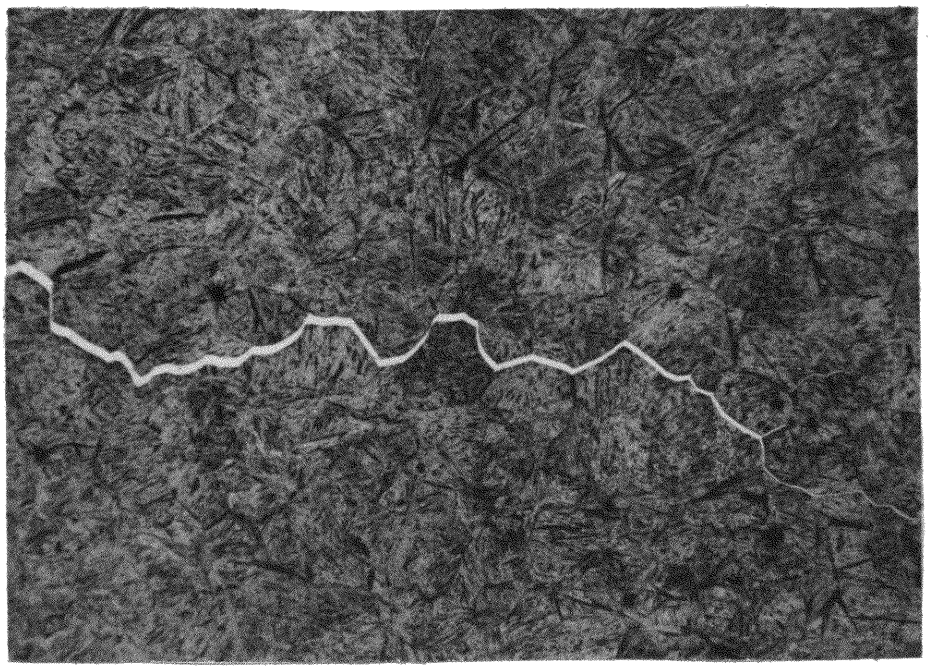

Figure 28. Photomicrograph showing liquid Cu penetration which led to rapid failure. Penetration perpendicular to surface of specimen. Nital etch. 150X

observed. In the absence of copper, although no tests were continued to failure, both plated and unplated samples showed no damage after 10,000 cycles in argon at 1100°C. Also no detrimental effects were ascribed to the copper after 10,000 cycles in tests run in argon and CO_2 at 1000°C, below the melting point of 1083°C for copper.

IV. DISCUSSION OF RESULTS

The observed effect of the increasing CO/CO_2 ratio can be entirely attributed to a decreasing oxygen potential in the gas phase. This, of course, implies that reaction II is insignificant in these results. That the zone, Figure 19, characteristic of the 100% CO tests might be due to a carbon pickup, is recognized. It is thought, however, that this zone is simply the result of the transformation of austenite to a product formed at higher temperature (i.e. ferrite + pearlite or bainite) which would be appropriate for a matrix zone depleted in the alloying elements which are known to be segregated in discrete particles. This description of the altered zone is favored since no carbon enhancement was observed and the zone was found to be softer than the matrix.

Assigning an oxygen potential to a 100% CO gas requires certain clarification. The gas consisted of CO entering the chamber but the instability of the gas resulted in deposition of carbon (soot) and generation of some CO_2. Carbon deposition at higher CO contents was common and traces of CO_2 were present in the exit gases of the 100% CO tests. This explains why the highest % CO points are not shown on the 100% CO line in Figure 9.

Oxide formation was observed on all specimens with greater than the equilibrium value of CO_2, as expected

from reaction I. These oxides were not magnetic, consequently wustite is assumed to be the predominate oxide form. A straight line fits the data (Figure 9) in the range of iron oxidation (>30% CO_2). The kinetics and mechanisms of the oxidation of iron in carbon monoxide-carbon dioxide atmospheres have been investigated by Smeltzer[24,25] and Petit, et al.[26,27] Initial oxidation was determined to be linear with the rate directly proportional to the partial pressure of CO_2 above the equilibrium value. Attempts at a more rigorous correlation between the rate of oxidation and the present results were unsuccessful because of insufficient data. It should be mentioned, however, that the mechanism of fracturing in the region of external oxidation is not a simple sequence of oxide formation, cracking of the brittle oxide exposing fresh surfaces, reformation of the oxide, etc. This mechanistic approach is eliminated on the basis of calculations using known rate constants which establish scale formation to be too slow to satisfy such an approach when applied to the results being reported herein. The explanation of Achter and co-workers[18,20,21] relies on surface adsorption of gaseous impurities resulting in a reduction of surface energy which facilitates crack propagation. After detailed studies of superalloys, Coffin[16,17,19] proposes that strain-induced oxidation is responsible for crack nucleation in the form of

wedge-shaped oxide intrusions. Crack propagation then takes place intergranularly because oxidation processes proceed more rapidly along these boundaries especially when under the influence of stress. Although the exact nature by which oxidation enhances cracking has not been established in the present investigation, the mechanism of cracking proposed to explain the results of this study is in basic agreement with that envisioned by Coffin.

Heretofore we have discussed only external oxidation. Indications are that the particles in the mottled zone are complex oxides of Fe, Cr, Mn and V which are formed by internal oxidation of the steel either with or without external formation of FeO. A schematic representation of the internal oxidation of iron alloys with small alloying additions is shown in Figure 29. Oxygen dissolved in the alloy will selectively oxidize the less noble component forming the internal precipitates which are probably complex Fe-X oxides. Chromium, manganese, and vanadium each form oxides which have larger negative free energy of formation values than iron oxides, thereby making their formation thermodynamically favored.[29] Internal oxidation indentical to that observed here has previously been reported to occur in similar low alloy steels subjected at high temperature to CO/CO_2 atmospheres.[30,31] In the present study the oxide precipitate is found in the matrix but prefers grain boundary formation.

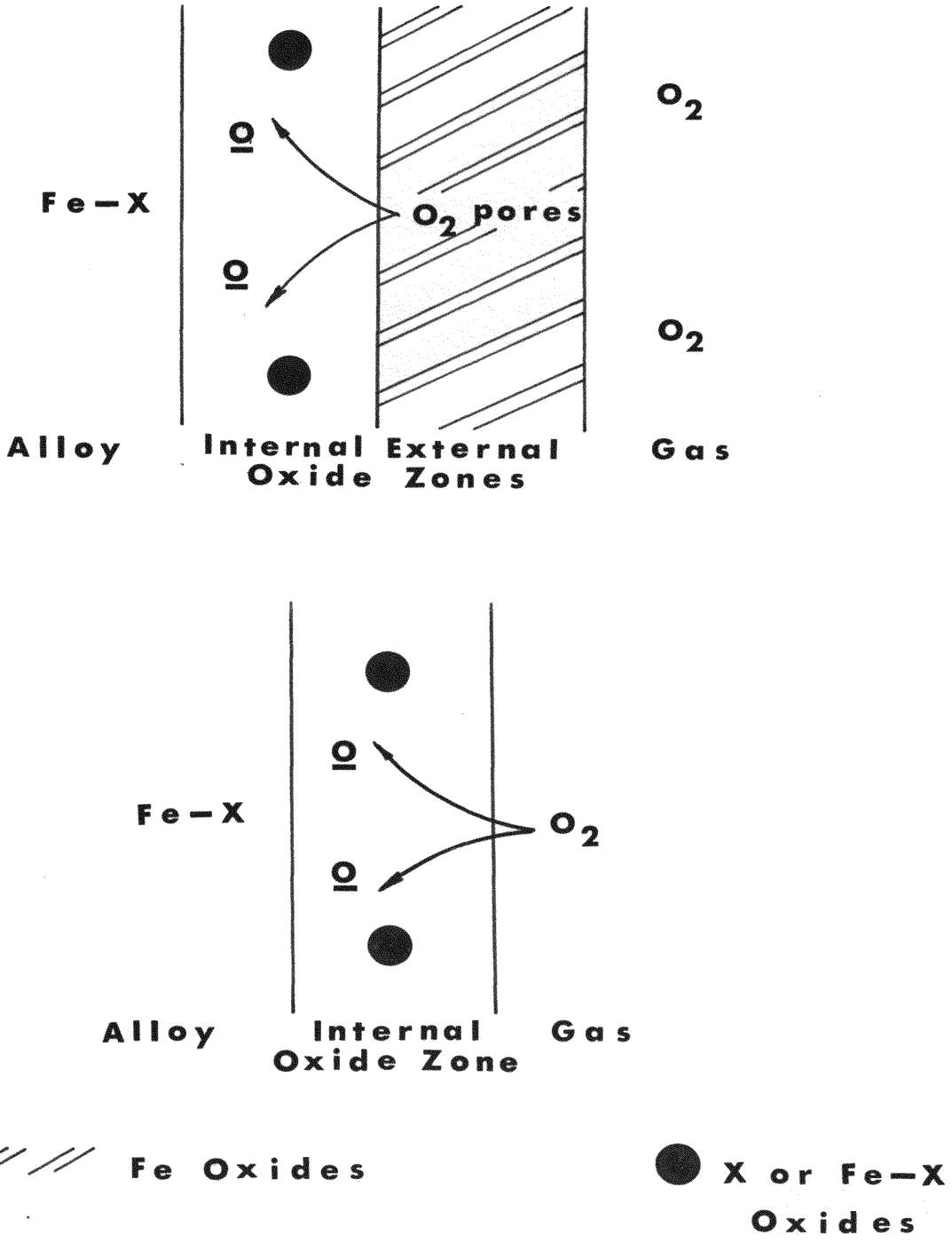

Figure 29. Representation of internal oxidation. (After Rahmel[28])

Meijering[32] rejects preferential penetration of oxides along grain boundaries during oxidation of iron. The dynamic stress conditions of the present tests compared to his static tests can easily account for this discrepancy.

Convincing evidence was presented which leads to the conclusion that cracking follows the grain boundary oxide precipitate (Figures 20 and 21). The effect on cracking of the internal oxide precipitate when distributed in the matrix is thought to be of secondary importance. It is possible that matrix precipitates may provide a form of oxidation strengthening, and retard crack initiation at the surface.

In discussing the effect of the Cr plating it will be helpful to represent the failure of a specimen by two stages, a crack initiation stage and a crack propagation stage. Manson[33] has treated high temperature failures in general and predicts that, at the temperature of the tests in this study, failures should be primarily intergranular with the initiation being a minor portion of the total life - the failure is propagation controlled. The role of the chromium plating in promoting cracking centers around the inherent defects in the plating. The crack initiation stage can be regarded as being intrinsic in the Cr plated specimens. However, tests carried out in argon suggest that this crack initiation is insignificant.

Since the cycles to failure for the plated and the unplated specimens are comparable in argon, it is concluded that failure in these tests was propagation controlled.

Contemplating the above previous paragraph, the premise that the effect of the plating in reducing the cycles to failure in an aggressive atmosphere is principally mechanical is invalid. Undoubtedly, cracks in the Cr assist in initiating cracks in the steel, but it is the combination of the existing crack and a chemical effect which is responsible for premature failure. The chemical contribution is the oxidation previously discussed. Correlation of the diffusion zone formation with cracking appears appropriate considering Figure 23, but the argon results seem to negate attaching any significance to the diffusion zone in the results of these experiments. In the unplated specimens the cycles to failure increase rapidly as CO_2 contents fall below that needed to maintain external oxidation. In fact, with very small amounts of CO_2, any effect of oxidation diminishes and the cycles to failure approach those of the inert atmosphere. In the Cr plated specimens, however, a positive effect of oxidation persists to very small quantities of CO_2. This is somewhat of an anomaly but can be explained by taking proper account of the chemical effect, as well as the mechanical effect. Apparently oxidation, particularly internal oxidation, has a minimal effect on cracking

behavior when distributed uniformly over the entire surface, but is detrimental when selectively formed at exposed areas beneath the cracks in the Cr. The increased stress in these areas is anticipated to be a primary factor in this behavior.

Liquid Cu grossly reduces the life of this steel due to a form of liquid metal embrittlement. According to Smith,[34] the formation of liquid films at the grain boundaries can be attributed to interfacial energy relationships which determine the dihedral angle θ, Figure 30. Applying energy values at 1105°C reported by Van Vlack[35] for liquid copper/austenite of 430 ergs/cm^2 and austenite/austenite of 850 ergs/cm^2 provides a dihedral angle approaching 0°. For this reason, the dramatic reduction of cycles to failure in the presence of a small amount of liquid copper observed in this study is to be expected. The tensile portion of each stress cycle greatly enhances penetration because it opens the properly oriented boundary offering a more favorable condition for penetration.

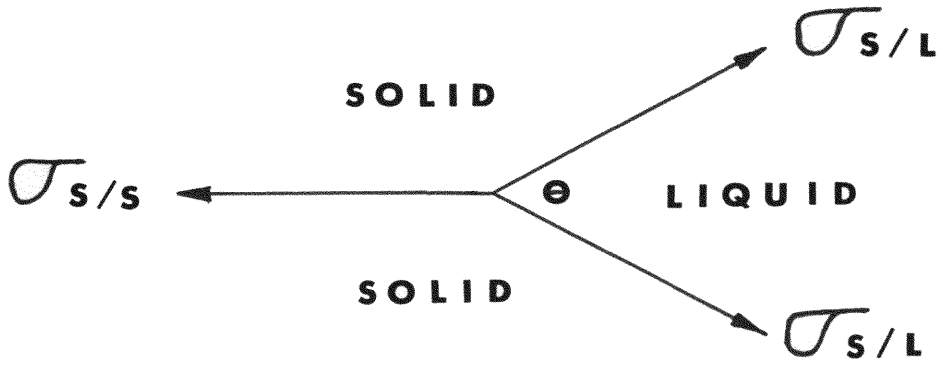

$$\sigma_{S/S} = 2\sigma_{S/L} \cos \theta/2$$

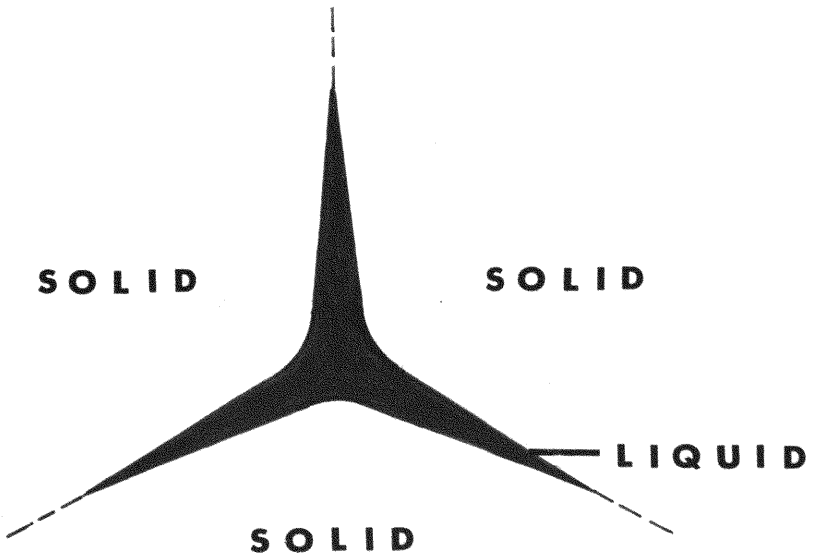

$$\theta \rightarrow 0^{\circ}; \quad \sigma_{S/S} \approx 2\sigma_{S/L}$$

Figure 30. Criteria for liquid metal penetration at grain boundaries. (After C. S. Smith[34])

V. SUMMARY

Initially, it must be remembered that the conditions of these tests do not exactly simulate the conditions existing in the gun barrel. A major difference is the kinetic factor with the rates experienced in gun barrels being orders of magnitude greater. It is assumed, however, that the trends observed in these laboratory experiments can be extrapolated to provide a better understanding of possible chemical changes in the gun barrel.

An obvious conclusion to the previous results is that if the copper deposits are liquid at any time, the resultant attack will be catastrophic. Futher firing tests on the 7.62 mm barrel excluding the copper cladding on the projectiles would definitely determine the effect of the copper.

The effect of the cracks in the Cr plating in enhancing chemical attack is probably more pronounced in these experiments than in the actual barrel. The same mechanism of concentrated chemical attack at the root of the existing crack would be operative in the Cr plated barrels so the conclusion is identical, i.e. cracking will be worse in Cr plated barrels. This does not imply that a plated barrel is inferior to the unplated barrel because the uniform wear of the unplated barrels has not

been accounted for. From these results it is apparent that a logical approach to minimize barrel deteriotation would be to develop crack-free platings. A less obvious, but perhaps more easily attainable, solution would be to incorporate a chemically resistant intermediate layer between the plating and substrate. These experiments indicate a major contribution of chemical effects in initiating the crack in the steel. Therefore, such a layer would retard propagation of the crack in the Cr into the steel.

The oxygen potential of the gaseous environment was shown to affect the cracking tendency. Certainly a low oxygen potential is desirable for minimizing deterioration of the barrel. Undetermined factors such as pressure, temperature, and gas composition which exist in the barrel make exact correlations to laboratory results impossible.

It is felt that the most important outcome of these experiments is the qualitative demonstration of how chemical reactivity affects gun barrel material behavior. This suggests alternate criteria for evaluation and selection of candidate materials for gun barrels. In addition to the normal thermal and mechanical properties, chemical resistance must also be considered.

BIBLIOGRAPHY

1. Hypervelocity Guns and the Control of Gun Erosion, NDRC Technical Report, Vol. 1, 1946.
2. Proceedings of the Interservice Technical Meeting on Gun Tube Erosion and Control, edited by I. Ahmad and J. P. Picard, Watervliet Arsenal, 1970.
3. R. C. Tooke and T. J. O'Keefe, A Metallurgical Study of Erosion in 7.62 mm Machine Gun Barrels, Final Report, DAAFO1-69C-0541, Rock Island Arsenal.
4. R. W. Gurry, Trans. AIME, 188, 678, (1950).
5. G. C. Wood, Oxidation of Metals, 2, 11 (1970).
6. R. A. Rapp, Corrosion, 21, 382 (1965).
7. Kofstad, High Temperature Oxidation of Metals, Wiley, 1966.
8. J. Chipman and E. F. Brush, Trans. AIME, 242, 35 (1968).
9. N. Bredz and H. Schwartzbart, Welding Journal, p. 305-S (1959).
10. G. Hume, L. H. Cope, and H. T. Hall, Metallurgia, April, 1965, p. 169.
11. A. E. Vainerman and A. A. Osetnik, Fig.-Khim. Mekh. Mat., 5, 151 (1969). Brutcher Translation 7981.
12. E. J. Eckel and S. J. Paprocki, Trans. ASM, 41, 1204 (1949).
13. Coles, Hill, Dawson, and Watson, Thermal and High Strain Fatigue, Institute of Metals, 1967, p. 270.

14. G. J. Hill, Thermal and High Strain Fatigue, Institute of Metals, 1967, p. 312.

15. E. Krempl and C. D. Walker, Fatigue at High Temperature, ASTM STP 459, p. 75 (1968).

16. L. E. Coffin, General Electric (Schenectady, N. Y.) Report 71-C-108 (1971).

17. L. E. Coffin, Trans. ASM, 56, 339 (1963).

18. M. R. Achter, G. J. Danek, and H. H. Smith, Trans. AIME, 227, 1296 (1963).

19. C. J. McMahon and L. E. Coffin, Metallurgical Trans. 1, 3443 (1970).

20. G. J. Danek, H. H. Smith, and M. R. Achter, Proc. ASTM, 61, 775 (1961).

21. P. Shahinian and M. R. Achter, Trans. AIME, 215, 37 (1959).

22. J. A. Webber, Carburizing, ASM Symposium, 1937, p. 89.

23. D. Shechtman and S. Niedzwiedz, Material Sci. and Eng. 5, 35 (1969).

24. W. W. Smeltzer, Acta Met., 8, 377 (1960).

25. W. W. Smeltzer, Trans. AIME, 218, 674 (1960).

26. F. S. Pettit and J. B. Wagner, Acta Met. 12, 35 (1964).

27. F. Pettit, R. Yinger, and J. B. Wagner, Acta Met. 8, 617 (1960).

28. A. Rahmel, Z. Elektrochem., 66, 363 (1962).

29. C. E. Wicks and F. E. Block, Thermodynamic Properties, Bureau of Mines Bull. 605 (1963).

30. I. S. Kozlovskii, Metal Science and Heat Treatment, 3, 157 (1967).

31. A. Hultgren and E. Hagglund, Trans. ASM, 39, 820 (1947).

32. J. L. Meijering, Acta Met., 3, 157 (1955).

33. S. S. Manson, Intl. Jnl. of Fracture Mech., 2, 327 (1966).

34. C. S. Smith, Trans. AIME, 175, 15 (1948).

35. L. H. Van Vlack, Trans AIME, 191, 1951, p. 251.

VITA

Robert C. Tooke was born April 11, 1941 at Cape Girardeau, Missouri. After education in the Cape Girardeau public schools, he attended the University of Missouri at Rolla and received the B.S. (1962) and M.S. (1966) degrees in Metallurgical Engineering. His professional career includes: Metallurgist, Bethelhem Steel Company, 1962-65; Instructor, UMR, 1967-72; Research Metallurgist, Army Weapons Command, intermittent 1967-1972; Manager-Quality Control, Bodine Aluminum, 1972-.

APPENDIX A

EXPERIMENTAL PROCEDURE

A. Apparatus

A laboratory apparatus was designed and constructed which permitted the high temperature testing of Cr-Mo-V gun steel under alternating stress in selected environments. An overall view of this apparatus has been shown in Figure 5. The essential elements of the apparatus are shown in the block diagram of Figure 31. The apparatus can be separated into functional categories consisting of: (1) test chamber; (2) induction heating unit; (3) stress application mechanism; (4) temperature control; (5) environment control. Each of these will now be described in detail.

1. Test chamber: The test chamber was a vacuum tight enclosure which contained the hot test specimen (described later) being alternately stressed (tension-compression) as a cantilever beam. A detailed drawing of the chamber with a specimen in place was previously shown in Figure 6. In addition to the forced air cooling of the entire chamber, it was necessary to water cool the top lid with a single loop of flattened 1/4" o.d. copper tubing. The joint between the plexiglass insulation plug and the induction coil leads was sealed with apiezon putty.

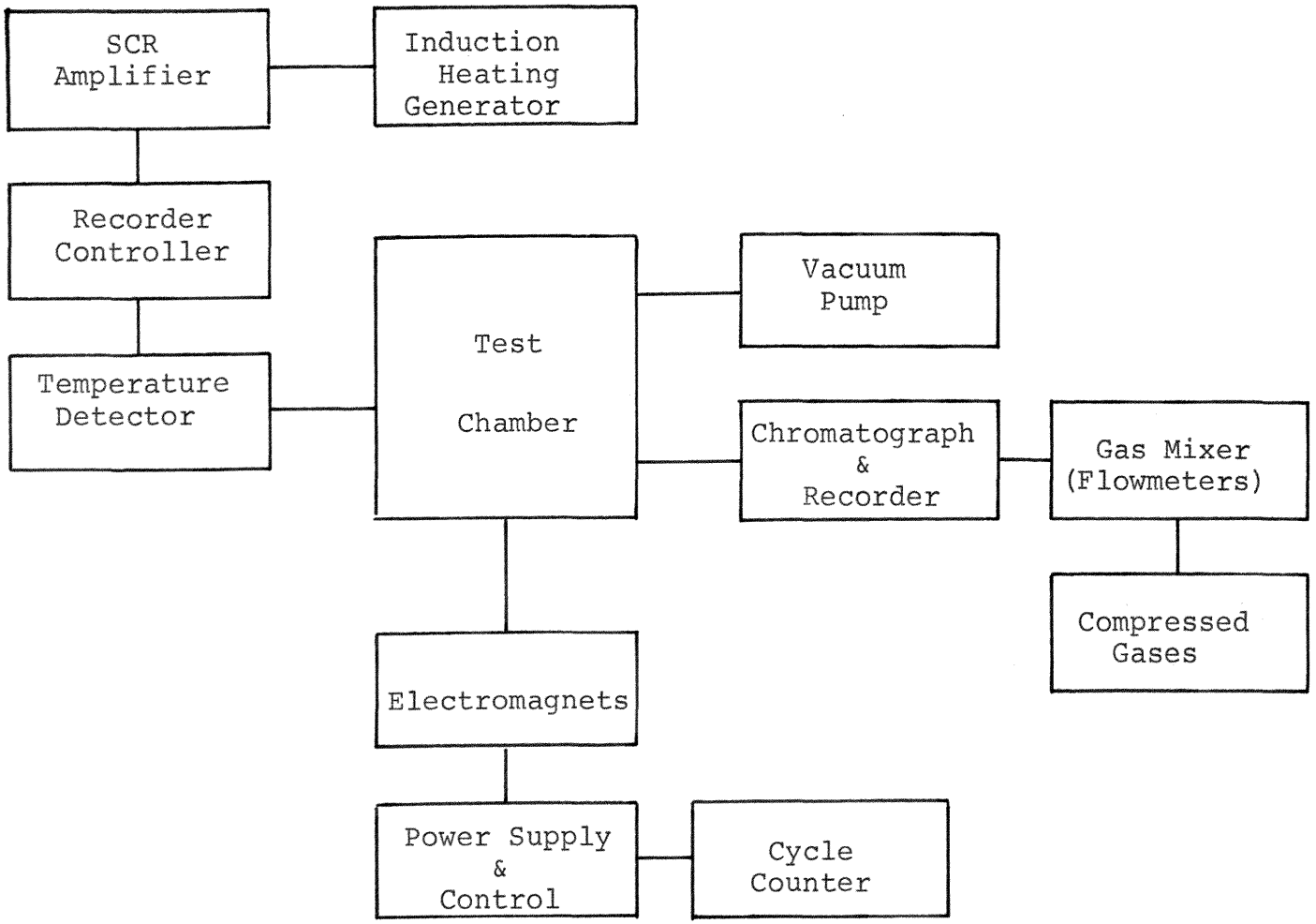

Figure 31. Diagram of apparatus Components.

2. Induction heating unit: A high frequency (450 kc) generator equipped with a saturable core reactor for output control coupled to a suitable coil provided for induction heating of the specimen. The generator was a Lepel Model T-5-3-KC-J-B with a maximum rated output of 5 KW. The coil used for heating the specimen was made from 3/16" o.d. copper tubing and contained four turns distributed over a total length of 1-1/4 inches. The coil is shown in Figure 32 with a heated specimen at 1000°C. Figure 33 contains representative temperature profiles for the specimen.

3. Stress application mechanism: A unique feature of the apparatus is the utilization of electromagnets to accomplish the desired stress pattern. Power was alternated via a DPDT relay between two diametrically opposite electromagnets thereby attracting the extension rod to first one side and then the other. The electromagnets required cooling by small blowers. The frequency of cycling was adjustable from 100 to 500 cycles per minute, one cycle being a complete tension-compression-tension sequence. An electrical impulse counter registered total cycles, this figure being checked against a timer showing elapsed time.

The extent of travel, i.e. the stress amplitude, was controlled by the stops in the fixture attached to the bottom plate of the test chamber (see Figures 6 and 32). The maximum stress can be calculated by:

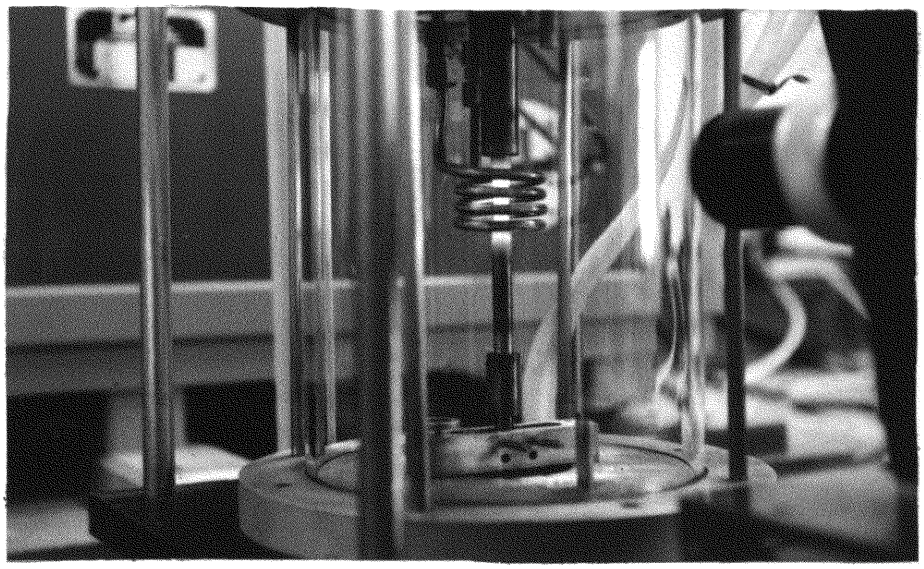

Figure 32. Induction coil with specimen at 1000°C.

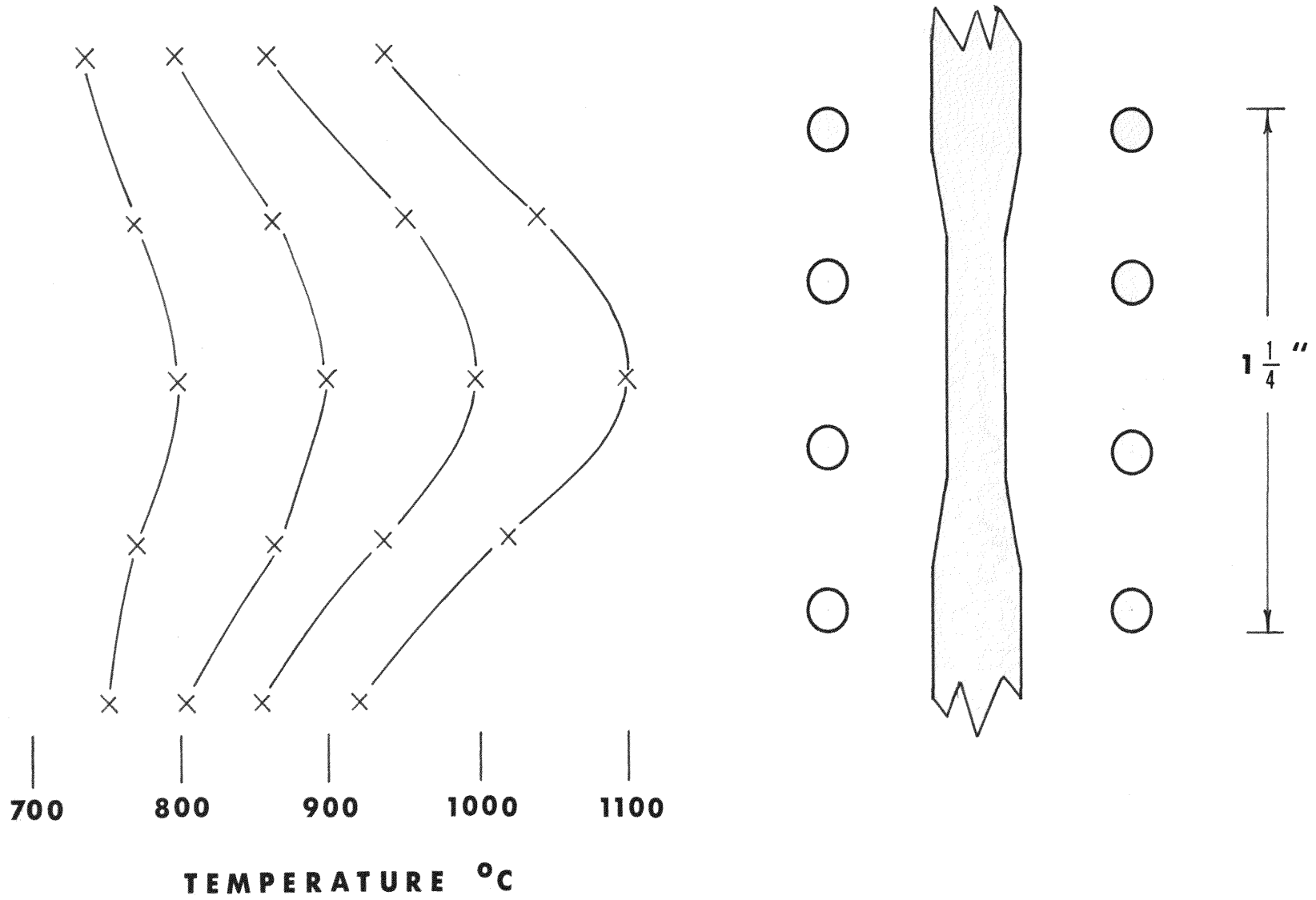

Figure 33. Temperature profiles in specimen heated in induction coil.

$$\sigma = \frac{3d \cdot E \cdot r}{l^2}$$

σ = stress

d = distance traveled before hitting stop

E = modulus of elasticity

r = radius of specimen (gage section)

l = distance from gage section to stops

Inserting the values of d = 1/16", E = 15 x 10^6 at 100°C, r = 0.1" and l = 3.7" into this equation yields a value for σ of 21,000 psi. This exceeds the yield strength for this material at 1000°C so the stress is in the plastic range. No attempt was made to determine the actual plastic strain involved in these experiments.

4. Temperature control: Temperature measurement was made with an Ircon Model 300T5C infrared radiation pyrometer and temperature indicating unit. An accessory fine focus lens was used which allowed accurate sighting of the pyrometer on a spot as small as .019 inches in the focal range 4-7 inches from the target. The 0-10 MV output from the above instrument was fed into a current adjusting recorder-controller (L & N Series 80). The interface needed between the output of the recorder-controller (0-5ma) and the input to the saturable core reactor (0-80v)

of the induction generator was provided by a L & N Series 11900 silicon controlled rectifier power package modified for an inductive load.

The development of a satisfactory temperature measuring procedure and calibration of the radiation pyrometer required considerable effort. Initial attempts to measure temperature directly on the surface of the specimen failed because changing surface conditions made it impossible to accurately determine the emittance value for the surface. Therefore, it was desirable to create a blackbody condition ($\varepsilon = 1$) by sighting the radiation pyrometer on a hole drilled in the sample.

The calibration of the radiation pyrometer involved comparison with temperature measured by a Pt-Pt 10% Rh thermocouple. Two holes were drilled in a 1/4" steel rod and a thermocouple was placed in one hole with Pt foil to provide good contact. The pyrometer was focused on the other hole. Agreement of the separately measured temperatures was obtained when an emittance setting of .92 was used which confirms the hole to be a good blackbody when the known loss of 8% through the glass walls of the test chamber is considered. Further confidence in this system of temperature measurement was obtained by observing the melting temperature of silver and copper foils placed in the hole. Copper (M.P. = 1083°C) was observed to melt at 1080°C. All of the previously described tests were

performed with the holes between the second and third turns of the coil. Temperature control during testing was achieved by focusing on a hole in the sample placed between the first and second turns of the coil so as not to interfere with the stress distribution in the gage section of the specimen (refer to Figure 35). This required the determination of temperature gradients which was accomplished by heating a specimen with two holes, one between the first and second turns, and the other between the second and third turns, allowing temperature equilibration, and measuring temperature at both holes. The results of this test are contained in Figure 34 which is the master graph used in all testing to determine the relationship between the set point or control temperature and the actual temperature in the gage section. Temperature accuracy is judged to be ±10°C at 1000°C.

5. Environment control: The atmosphere of the reaction chamber was established through the use of high purity compressed gases of argon (99.996%), carbon monoxide (99.7%) and carbon dioxide (99.9%). The test chamber was evacuated prior to the introduction of the gases then re-evacuated after backfilling with the desired gas mixture. When using argon, the reaction chamber was filled with the gas and the test was made under static conditions after venting the gas during heating. When CO, CO_2, or mixtures of these gases were used the flowrate

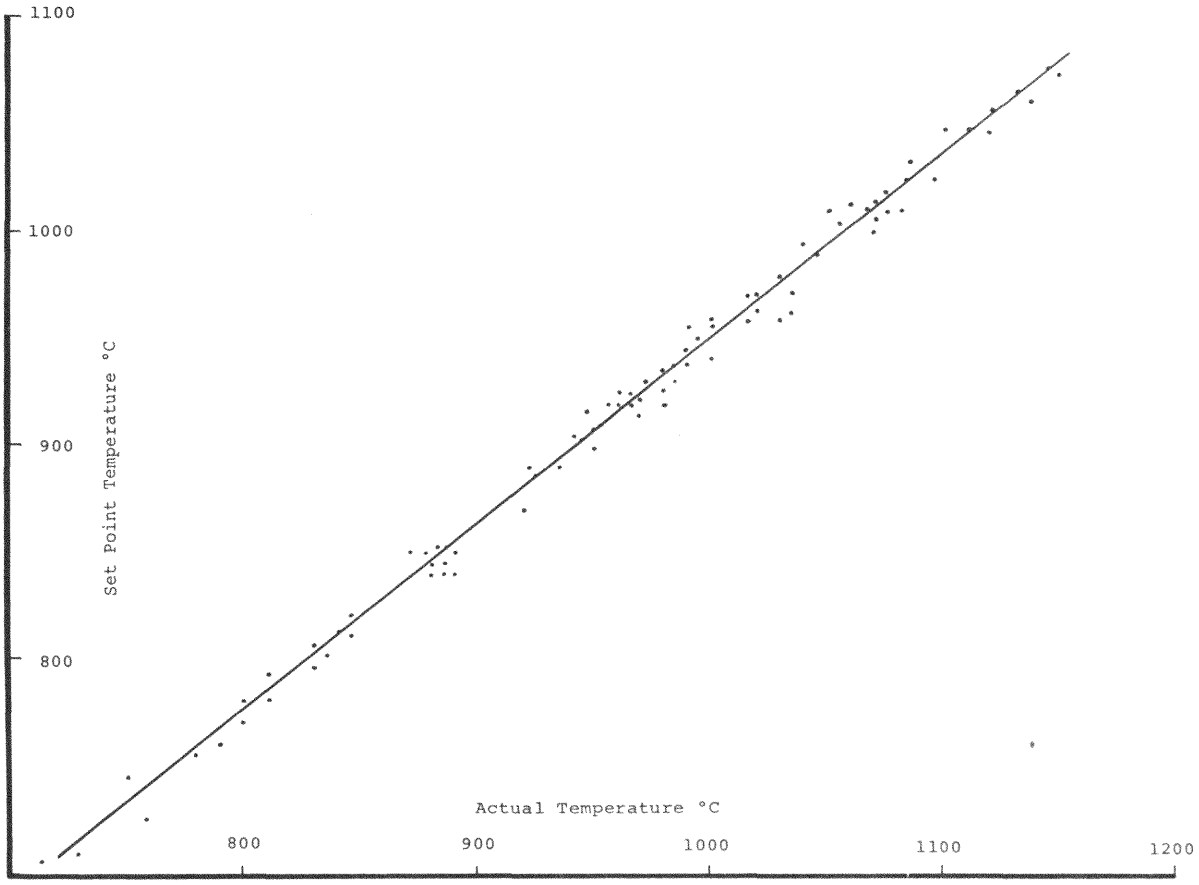

Figure 34.

Temperature Calibration Curve

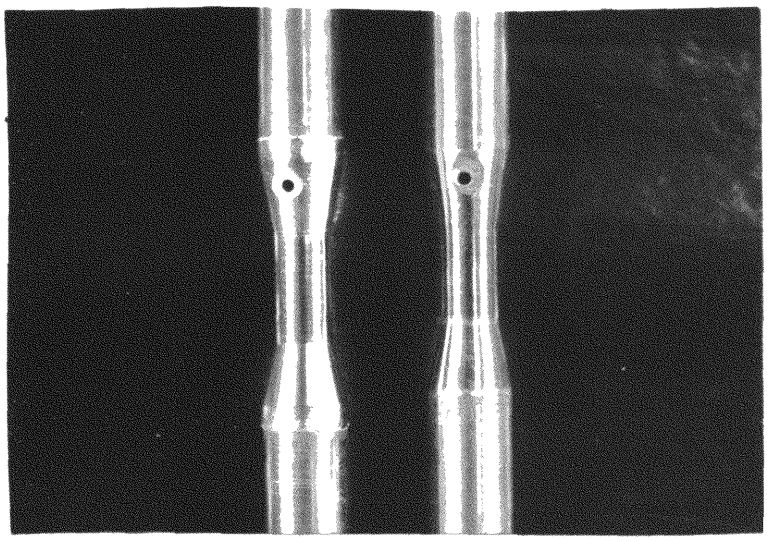

Figure 35. Gage section of test specimens, right - unplated; left - Cr plated.

was 40 cc/min. The flowrate and mixing of the gases was governed by Matheson Model 665 Gas Proportioner which blended the gases by individual flowmeters. All gas mixtures were checked and recorded with a Fisher Gas Partitioner (Model 25V) and a Texas Instruments Servoriter II recorder. Gas samples for analyses were obtained through an integral gas sampling valve. Provisions for analysis of exit gases was also available. All CO/CO_2 mixtures were burned after exit from the test chamber.

B. Specimen Preparation and Test Procedure

Two types of test specimens, Cr plated and unplated, were incorporated in the high temperature studies both of which are represented in Figure 35. All specimens were machined from forged stock from the same heat of Cr-Mo-V steel. A check analysis gave the following composition:

C	Mn	Si	Cr	Mo	V
0.43	0.97	0.29	1.29	0.65	0.21

The non-metallic inclusion orientation was elongated in the axial direction of the specimens. After machining the specimens were finished to a 600 grit surface with emery paper. Unplated specimens were finished to a gage section diameter of .200" ±.001" while the specimens to be plated were finished to a diameter of .192" ±.001" and subsequently received a standard electrolytic hard chromium plating of a thickness of .003" to .004". A hole, .225"

deep and .045" diameter was drilled on the taper of each specimen for temperature measuring purposes as described previously. The specimens were thoroughly cleaned with acetone before using.

Preparation for a typical test included closing the test chamber after assembly of the test specimens, evacuating, backfilling with the desired gas, re-evacuating, and allowing the gas to flow for 15 minutes. At this time the specimen was heated to the test temperature (generally 1000°C) which required less than 60 seconds and cycling was begun. Most tests were carried to failure. Copper was placed on the designated specimens by melting a fine copper wire in situ at 1100°C in argon and allowing 15 seconds for the Cu to flow over the surface before proceeding with the test. The liquid copper readily spread over both the steel and Cr plated surfaces.